Unentangled Vitrimer Melts: Interplay between Chain Relaxation and Cross-link Exchange Controls Linear Rheology

Ralm Ricarte*,† and Sachin Shanbhag*,‡

†*Department of Chemical and Biomedical Engineering, FAMU-FSU College of Engineering, Tallahassee, FL 32310.*

‡*Department of Scientific Computing, Florida State University, Tallahassee, FL 32306*

E-mail: rricarte@eng.famu.fsu.edu; sshanbhag@fsu.edu

Phone: +1 (850) 410-6170; +1 (850) 644-6548

Abstract

Vitrimers are polymer networks that engage in dynamic associative exchange reactions. Their covalent cross-links preserve network connectivity but permit topology fluctuations, making them both insoluble and processable. Here, we use a sticky Rouse model approach to elucidate structure-viscoelasticity relationships for unentangled vitrimer melts. Two different versions of the sticky Rouse model are explored: the simplified sticky Rouse (SSR) and the inhomogeneous Rouse (IHR). Unlike the SSR, the IHR model accounts for interactions between slow modes that arise due to cross-linking and fast Rouse modes of the underlying polymer chain. First, we identify the conditions where the SSR sufficiently approximates the IHR. Then, we use the IHR to explore the influence of structure and temperature on the zero-shear viscosity (η_0) and characteristic relaxation time (τ^*). Vitrimers with uniform and random cross-link distributions exhibit larger η_0 and τ^* than gradient and blocky types. Polydimethylsiloxane vitrimer (which has a flexible backbone) shows an Arrhenius temperature dependence

for η_0, while polystyrene vitrimer (which has a rigid backbone) is only Arrhenius at high temperatures. For stress relaxation measurements, the short time dynamics represent monomer friction, while the long time dynamics encompass a combination of network strand relaxation and cross-link exchange. Due to the different temperature dependences of the processes, time-temperature superposition fails. The effective rheological activation energy can be estimated a priori from the cross-link exchange activation energy and backbone Williams-Landel-Ferry parameters. Finally, we discuss the utility and limitations of the sticky Rouse approach for studying vitrimer viscoelasticity, and best practices for measuring η_0 and τ^*.

1 Introduction

Vitrimers are covalently cross-linked polymer networks that are insoluble in a good solvent, yet still flow at elevated temperatures.[1–5] These paradoxical traits – a combination not found in other types of polymers – are enabled by their cross-links, which engage in thermoactivated associative exchange reactions that cause the network topology to fluctuate. In contrast to networks with dissociative cross-links, whose cross-link (XL) density follows an equilibrium relationship with temperature and concentration,[3,6,7] vitrimers maintain network connectivity and XL density at all times and temperatures below degradation conditions.[1–5,8] Conversion of a polymer to a vitrimer imparts it with improved solvent resistance and mechanical strength (like a thermoset) but does not compromise its ability to be processed by extrusion or other conventional techniques (like a thermoplastic).[9–17] This marriage between high-performance and processability inspires significant interest into vitrimer structure-property relationships and applications.[2–5] Here, we demonstrate a generalized Rouse model approach for relating the molecular structure of a vitrimer and its corresponding linear viscoelasticity.

The current framework for interpreting vitrimer rheology originates from the seminal epoxy vitrimer studies of Montarnal, Leibler, et al.[1,18–20] For these materials, epoxy networks featuring β-hydroxy esters were doped with metal or organic catalyst. While at room temperature the vitrimers behaved as classical thermosets, at elevated temperatures the β-hydroxy esters underwent transesterification, allowing the epoxies to fully relax stress but still remain insoluble. The transient relaxation modulus was described by a simple Maxwell exponential decay, while the zero-shear viscosity and terminal relaxation times followed an Arrhenius relationship with temperature. The apparent activation energies estimated from these rheological properties (E_a^{rh}) were consistent with the activation energy for transesterification of small molecule epoxy analogues (E_a^{sm}). Extrapolation of the Arrhenius relationship provided T_v, the temperature at which the vitrimer viscosity equals 10^{12} Pa s – an empirical threshold for processability. Alteration of catalyst type tuned E_a^{rh}, while variation of the epoxy network chemical composition changed the glass transition tempera-

ture (T_g).[1,18–20]

Following these initial studies, researchers have generally focused on two different strategies for modifying vitrimer flow and mechanical properties: (i) altering the cross-linker exchange reaction chemistry to tune E_a^{rh} or (ii) varying the vitrimer backbone flexibility to change T_g. For the cross-linker, efforts over the past decade have created a vast library of externally and internally catalyzed associative exchange reactions that may be incorporated into vitrimer networks. Such chemical properties as cross-linker structure,[21–26] reactive functional group stoichiometry,[17,27–31] catalyst loading,[1,17,18,32] catalyst pK_a,[33] and even coordination between cross-linker and catalyst modulate the E_a^{rh} and rheological profile.[34] For the backbone, the vitrimer concept has been adapted to a wide variety of commodity polymers, including those with high T_g,[9,10,12,16] moderate T_g,[27,35,36] low T_g,[21,29,37–39] or semi-crystallinity.[40–42] Inclusion of branching,[43–46] macro/microphase separation,[12,13,47–49] or additives within the vitrimer matrix offers additional design parameters.[50–53]

While the synthetic toolset for vitrimers has grown quite sophisticated, understanding vitrimer thermorheological properties remains primitive. Vitrimers that exhibit an Arrhenius temperature dependence generally express an E_a^{rh} that is larger than E_a^{sm}. Röttger et al. found that the E_a^{rh} of poly(methyl methacrylate) vitrimers with dioxaborolane XLs was $\sim$ 80 kJ/mol, much larger than the E_a^{sm} = 15 - 30 kJ/mol observed for small molecule dioxaborolanes undergoing metathesis.[9,22] Lessard et al. and Spiesschaert et al. demonstrated that the ratio of E_a^{rh} to E_a^{sm} for vitrimers with vinylogous urethane XLs is a function of the backbone chemistry.[15,16,54] Moreover, the stress relaxation of vitrimers near their T_g deviates from the simple Maxwell model.[2] At this temperature regime, secondary plateaus and peaks commonly appear in small amplitude oscillatory shear measurements,[29,55,56] alluding to the presence of additional relaxation modes and timescales. The observed relationship between the XL density and terminal relaxation time also varies drastically across systems.[38,54,57]

These complexities of vitrimer flow behavior motivate several theoretical approaches for understanding the rheology. Terentjev et al. pioneered the development of microscopic constitutive equations to describe vitrimer stress relaxation, creep, and uniaxial deformation. Their theories high-

lighted the strong influence of the cross-linker exchange kinetics on the material response.[44,45,58–60] Qi et al. used finite element modeling to relate cross-linker exchange to the stress distribution in vitrimers during deformation and surface welding.[61–66] Wu et al., Jourdain et al., and Fang et al. employed time-temperature superposition to collapse rheological data into master curves. In these works, superposition was not achieved over the entire relaxation spectrum, hinting that the systems had multiple relaxation modes with differing timescales and temperature dependences.[56,67,68] In addition to continuum methods, molecular dynamics (MD) and Monte Carlo (MC) simulations provide deep insight into the relationship between structure and flow. Although the wide range of timescales in vitrimer systems makes it difficult to use standard atomistic molecular simulations, Perego and Khabaz overcame this barrier by employing hybrid MD/MC simulations to study expansion and chain diffusivity around T_v.[69] Using coarse-grained MD, Sciortino et al. found that the macroscopic vitrimer viscosity is a reflection of both network topology and cross-linker exchange kinetics.[70–72] Coarse-grained slip link modeling also offers a pathway to interrogate the interactions between backbone relaxations and transient cross-linking.[73]

On a broader scale, vitrimers can be considered to be a subset of dynamically cross-linked polymer networks, for which several rheological theories have been already developed. The history of characterizing these networks can be traced back to the transient network model of Green and Tobolsky.[74] Inspired by the theory of rubber elasticity, they proposed this model for polymer melts in which entanglements were treated as temporary junctions that could break and reform spontaneously.[74] The basic formalism of transient networks was extended, generalized,[75,76] and specialized for physically cross-linked networks and associating polymers.[77–79] For unentangled polymers, Baxandall demonstrated that at long timescales, the dynamics of reversibly cross-linked chains follow Rouse dynamics.[80,81] Leibler, Rubinstein, et al. comprehensively fleshed out the gelation and dynamic properties of reversible networks for unentangled ("sticky Rouse") and entangled ("sticky reptation") chains using scaling theory as their primary tool.[82–85] The resulting framework is quite powerful and precisely portrays the dynamics of many complex polymeric systems, including ionomers,[86,87] supramolecular polymers,[88–90] complex coacervates,[91–93] and

polymer-protein conjugates.[94]

In this work, we employ the sticky Rouse model to investigate the linear viscoelasticity of monodisperse unentangled vitrimer melts. We focus on fully developed networks beyond the gel point, where the sticky Rouse model is ideally suited. We employ both a generalized sticky Rouse model - labeled the inhomogeneous Rouse model (IHR) - and a simplified sticky Rouse model (SSR) that provides an approximate solution. The questions we seek to address are the following:

1. Under what conditions does vitrimer rheology follow an Arrhenius temperature dependence?

2. What is the relationship between E_a^{rh} and E_a^{sm} ? How does the molecular structure, backbone flexibility, and cross-linker chemistry affect this relationship?

3. What are the potential pitfalls of using approximate methods to determine the zero-shear viscosity (η_0) and characteristic relaxation time (τ^*) in estimating E_a^{rh} from Arrhenius plots?

4. When do the IHR and SSR converge and diverge? What are the relative merits of one over the other?

Using the IHR and SSR to simulate the linear viscoelasticity of model vitrimers, we find that the rheology is a product of chain friction and Arrhenius contributions, signifying the interplay between network strand relaxation and XL exchange. The different temperature dependences of the chain friction and Arrhenius modes leads to a breakdown of time-temperature superposition. XL density, kinetics, and distribution control both η_0 and τ^*. Furthermore, the relationship between E_a^{rh} and E_a^{sm} depends on the chain friction and temperature window explored. E_a^{rh} can even be estimated based solely on knowledge of the E_a^{sm} and Williams-Landel-Ferry parameters of the backbone. The presence of a pre-exponential factor in the model also offers an avenue for evaluating the mobility and mechanism of exchange of XLs within a vitrimer matrix. These findings not only provide insight into fundamental vitrimer structure-viscoelasticity relationships, but also highlight the importance of using rigorous practices to determine η_0, τ^*, and E_a^{rh} from rheological measurements.

2 Methods

As shown in figure 1a, we consider a bead-spring chain with N beads, of which N_x beads are sticky. For vitrimers, these sticky beads correspond to associative XLs. We focus on fully developed vitrimer networks of unentangled polymer melts whose XL density is above the gel point. Thus, $N \lesssim N_e$, where N_e is the number of monomers in an entanglement strand, and $N_x \geq 2$, where N_x is the average number of XLs per chain.

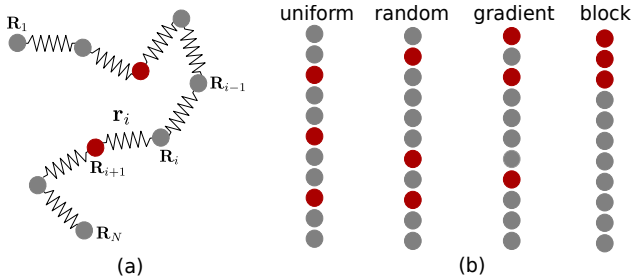

Figure 1: (a) Schematic diagram of a bead-spring chain with N monomers, of which $N_x = 2$ are sticky (red beads). (b) Four different distributions of sticky beads are considered: uniform, random, gradient, and block (see descriptions in text). For each distribution type, the sample chains have $N = 11$ and $N_x = 3$.

2.1 Standard Rouse Model

For the standard Rouse model, the chain has $N - 1$ springs with spring constant $k = 3k_BT/b^2$, where k_B is Boltzmann's constant, and b is the statistical segment length. The beads are located at $\mathbf{R}_i$, where $i = 1, 2, \cdots, N$. The spring end-to-end vectors $\mathbf{r}_i = \mathbf{R}_{i+1} - \mathbf{R}_i$ for $i = 1, 2, \cdots, N-1$.

The equation of motion is controlled by spring and Brownian forces.[95,96] These can be cast as a coupled set of equations for the springs,

$$\dot{\mathbf{r}}_i + \sum_{j=1}^{N-1} C_{ij}\mathbf{r}_j = \mathbf{f}_i^B, \qquad i = 1, 2, \cdots, N-1, \tag{1}$$

where $\mathbf{f}_i^B$ is the Brownian force that satisfies the fluctuation-dissipation theorem. The tridiagonal matrix $\mathbf{C}$ encodes the connectivity of the springs. For the standard or "homogeneous" Rouse model

without any sticky beads ($N_x = 0$), $C_{ij} = (k/\zeta)\, A_{ij}$, where

$$A_{ij} = \begin{cases} 2 & \text{if } i = j \\ -1 & \text{if } i = j \pm 1 \\ 0 & \text{otherwise.} \end{cases} \tag{2}$$

The ratio of the bead friction and spring constant, $\tau_b = \zeta/k$, is a natural timescale associated with bead or monomer relaxation. The eigenvalues of the matrix $\mathbf{C}$ are inversely proportional to spectrum of relaxation times,

$$\lambda_i = \frac{4k}{\zeta} \sin^2\left(\frac{i\pi}{2N}\right), \qquad i = 1, 2, ..., N-1. \tag{3}$$

The Rouse stress relaxation time is half the end-to-end vector decorrelation time because it is obtained from a quadratic function of the amplitude of the normal modes.[97] Thus, $\tau_i = 1/(2\lambda_i)$, which implies,

$$\tau_i = \frac{\zeta}{8k \sin^2(i\pi/2N)} = \frac{\tau}{\sin^2(i\pi/2N)}, \qquad i = 1, 2, ..., N-1, \tag{4}$$

where $\tau = \tau_b/8$ is the elementary Rouse timescale.

For $N \gg 1$, the relation $\sin x \approx x$ is invoked to obtain the approximate spectrum (denoted by "hat"),

$$\hat{\tau}_i = \frac{\tau_1}{i^2} = \frac{\zeta}{2\pi^2 k}\left(\frac{N}{i}\right)^2, \qquad i = 1, 2, ..., N-1, \tag{5}$$

where $\hat{\tau}_1 = \hat{\tau} N^2$, and $\hat{\tau} = \tau_b/(2\pi^2)$. Note that the true and approximate spectra are equal only for the slow modes ($i \ll N$). In particular, $\tau_1 \approx \hat{\tau}_1$, but the elementary timescale $\tau \neq \hat{\tau}$. Instead, $\tau/\hat{\tau} = \pi^2/4 > 1$. In the limit of large times, slow modes dominate the stress response. The difference in the spectrum at short timescales does not materially affect the $G(t)$ calculation given

by,

$$\phi(t) = \frac{G(t)}{G_0} = \frac{1}{N}\sum_{j=1}^{N-1} e^{-t/\tau_j}, \tag{6}$$

with modulus $G_0 = \rho RT/M_0$, where ρ is the density of the polymer melt, R is the universal gas constant, and M_0 is the molar mass associated with a bead. The zero-shear viscosity is given by,

$$\eta_0 = \int_0^\infty G(t)\, dt = \frac{G_0}{N}\sum_{i=1}^{N-1} \tau_i. \tag{7}$$

The timescale τ_η associated with η_0 is given by the ratio of the viscosity and modulus, $\tau_\eta = \eta_0/G_0$. From eqn 7, τ_η can be interpreted as the *average relaxation time*. Due to the dispersion in Rouse relaxation times, it is biased towards slow modes. For the standard Rouse model, if we approximate $\tau_i = \hat{\tau}_i = \hat{\tau}(N/i)^2$, and consider the limit of large N,

$$\tau_\eta^R \approx \frac{\hat{\tau}N^2}{N}\sum_{i=1}^{N-1}\frac{1}{i^2} \approx \frac{\tau_b N}{2\pi^2}\left(\frac{\pi^2}{6}\right) = \frac{N\tau_b}{12}. \tag{8}$$

This reflects the classic $\eta_0 \sim N$ dependence, which is indeed observed empirically for short unentangled polymer melts. Note that τ_η^R, which represents an average over all the timescales in the Rouse spectrum, is linear in N, while the longest relaxation time $\tau_1 \sim N^2$. Depending on the use case, the characteristic relaxation time τ^* may be identified with either τ_η or τ_1. Experimentally, τ_η is obtained simply from the ratio of the viscosity and modulus, while τ_1 has to be calculated by fitting a discrete relaxation spectrum to the data.[98–102]

2.2 Sticky Rouse Model

For the sticky Rouse model, the key idea is to incorporate the lifetime of a XL by increasing the frictional drag associated with sticky beads. Thus, the terms XL and sticky bead are used interchangeably in this paper. Furthermore, we assume that XLs are fully saturated, i.e., there are no unpaired sticky beads.

Unlike many dynamically cross-linked systems where the XL density changes as a function of

temperature or concentration, the total number of XLs in vitrimers is strictly conserved. Dynamical changes in network structure are mediated by exchange reactions, rather than breakage and reformation of XLs. Due to the symmetry of XL exchange reactions, and the assumption of saturation of XLs, the number and location of sticky beads on participating chains is preserved. This makes the sticky Rouse model particularly well-suited. Furthermore, since the number of XLs is baked in at synthesis, N_x is independent of temperature. We entertain two different versions of the sticky Rouse model: the inhomogeneous Rouse (IHR) model and the simplified sticky Rouse (SSR) model.

2.2.1 Inhomogeneous Rouse Model

The IHR model is a generalization of the standard or homogeneous Rouse model. It relaxes the constraint of uniform spring constants and drag coefficients; therefore, $k_i \neq k$ and $\zeta_i \neq \zeta$, where k_i is the spring constant of the i^{th} spring, and ζ_i is the drag coefficient of the i^{th} bead. This model was initially proposed by three different groups, nearly simultaneously, to predict the linear rheology of amorphous mixtures of block polymers.[103–105] In these studies, the difference between the two blocks was represented as a difference in friction coefficients. Similar versions of the theory were also used to study bidisperse homopolymer melts with short and long chains,[106] and to investigate the eigenmodes of relaxation in associating polymers.[107]

In the IHR model, the equation of motion is still governed by eqn 1, albeit with a more general tridiagonal matrix $\mathbf{C}$. For $i = 1, 2, ..., N-1$, the nonzero elements of $\mathbf{C}$ are given by,

$$\begin{aligned} C_{i,i-1} &= -k_{i-1}/\zeta_i \\ C_{i,i} &= k_i/\zeta_i + k_i/\zeta_{i+1} \\ C_{i,i+1} &= -k_{i+1}/\zeta_{i+1}, \end{aligned} \tag{9}$$

assuming $k_0 = k_N = 0$, in these expressions. In this work, we set $k_i = k = 3k_BT/b^2$, assuming that all the beads (regular or sticky) are separated by the same average distance b. The frictional

drag associated with the N_x sticky beads is denoted by ζ_x; similarly the drag associated with the remaining $N - N_x$ regular beads is denoted by ζ. The eigenvalues of $\mathbf{C}$ can be numerically evaluated to obtain the spectrum of $N - 1$ relaxation times, $\tau_i = 1/(2\lambda_i)$,[107,108] from which the stress relaxation response can be obtained using eqn. 6.

2.2.2 Simplified Sticky Rouse Model

For the simplified sticky Rouse (SSR) model, an approximate solution is obtained when the sticky and regular Rouse modes are well-separated ($\zeta_x \gg \zeta$), and the number of XLs/chain is sufficiently large ($N_x \gg 1$). The SSR model asserts that the stress relaxation of unentangled monodisperse associating polymers contains two sets of non-interacting Rouse-like contributions,[80,82,86,109]

$$\phi(t) = \frac{G(t)}{G_0} = \frac{1}{N}\left[\sum_{j=1}^{N_x-1} \exp\left(-\frac{j^2 t}{\tau_x N_x^2}\right) + \sum_{j=N_x}^{N-1} \exp\left(-\frac{j^2 t}{\tau N^2}\right)\right]. \tag{10}$$

The first summation contains slow sticky modes that arise due to XL exchange, and the second summation includes fast Rouse modes of the underlying polymer chain. Here, the timescales τ_x and τ are related to the viscous drag, ζ_x and ζ, associated with the sticky and regular Rouse beads (figure 1a), respectively. As demonstrated in sec. 3.1, under certain conditions, the SSR model is an excellent approximation to the IHR model.

It is helpful to highlight the differences between the two versions of the sticky Rouse model considered here. Unlike the SSR model, the IHR model does not regard the regular and sticky modes as independent contributions that can be summed up. Instead, it considers a single Rouse chain where the slow and fast modes are free to interact. The expression for the Rouse time $\tau_x N_x^2$, corresponding to the XLs in the SSR, implicitly assumes $N_x \gg 1$, which may not be true for lightly cross-linked chains. Furthermore, the response of the IHR can account for different distributions of sticky beads along the chain. As shown later, when $N_x \gg 1$, $\tau_x N_x^2 \gg \tau N^2$, and the XLs are distributed uniformly or randomly, the IHR and SSR models agree with each other. Thus, the SSR can be thought of as a special case of the IHR, which is convenient to use under appropriate

conditions.

2.3 Distribution of XLs

Here we consider four different distributions of sticky beads, as depicted schematically in fig. 1b: (i) uniform, (ii) random, (iii) gradient, and (iv) block. Note that we do not account for composition fluctuations or microphase separation, essentially assuming that the χ-parameter characterizing the enthalpic interaction between regular and sticky beads is zero.

For *uniform distribution*, we determine the spacing $\Delta N = (N+1)/(N_x+1)$. When possible, N and N_x are selected so that ΔN is an integer; otherwise ΔN is rounded to the nearest integer. The location of the sticky beads is marked as $j\Delta N$, where $j = 1, 2, \cdots, N_x$. In the example shown in fig. 1b, $N = 11$ and $N_x = 3$; thus, $\Delta N = (11+1)/(3+1) = 3$, and beads 3, 6, and 9 are marked as sticky beads. This protocol is deterministic: a particular choice of N and N_x uniquely determines the architecture of the sticky Rouse chain.

For *random distribution*, we consider each bead along the chain in turn. With a constant probability $\rho_x = N_x/N$, it is marked as a sticky bead; otherwise it is marked as a regular bead. Since this protocol is stochastic, the number of XLs on any particular chain n_x may deviate from the prescribed N_x, and is binomially distributed,

$$\pi(n_x; \rho_x, N) = \binom{N}{n_x} \rho_x^{n_x} (1-\rho_x)^{N-n_x}. \tag{11}$$

For the random distribution of XLs, we average the response over an ensemble of 1000 chains.

For *gradient distribution*, the probability ρ_x^i of marking a bead i as sticky is not constant. Instead, it increases from one end to the other. Thus, we set $\rho_x^1 = 1$, and $\rho_x^N = 0$. For internal beads, we assume a form,

$$\rho_x^i = \left(\frac{N-i}{N-1}\right)^{\alpha}, \tag{12}$$

where α is determined by requiring the average or expected number of XLs per chain to equal N_x,

$$\sum_{i=1}^{N} \rho_x^i = \sum_{i=1}^{N} \left(\frac{N-i}{N-1} \right)^{\alpha} = N_x. \tag{13}$$

The value of α is determined numerically, and for large N and N_x, it is usually close to $\alpha \approx \rho_x^{-1} - 1$. Note that the method is stochastic, and like random distributions, we average the response over an ensemble of chains.

Block distribution can be thought of as an extreme case of gradient distribution, where all the sticky beads are concentrated at one end. Therefore, $\rho_x^i = 1$ for $i = 1, \cdots N_x$, and $\rho_x^i = 0$, for $N_x < i \leq N$. Block and uniform distributions are deterministic, while the other two distributions are not. One can think of random distribution as a stochastic perturbation of the uniform distribution. Similarly, one can think of gradient distribution as intermediate between random and block distributions.

2.4 Cross-link Frictional Drag

Since the lifetime of a XL is governed by a chemical reaction, it follows an Arrhenius relation,[110]

$$\tau_x = \tau_x^0 e^{E_a^{\text{sm}}/RT} \tag{14}$$

where E_a^{sm} is the activation energy for the chemical reaction, and τ_x^0 is the pre-exponential factor. In the homogeneous Rouse model the timescale $\tau \sim \zeta/k$. Since $k \sim k_B T/b^2$ is assumed to be uniform, it implies $\zeta \sim \tau$ and $\zeta_x \sim \tau_x$. However, based on scaling arguments for the self-diffusivity of chains, we can derive a more general expression for the usual scenario where $\tau_x > \tau$.

First, we recap the argument presented by Colby et al.[111] The diffusivity D_0 of a Rouse chain without XLs ($N_x = 0$) with relaxation time $\mathcal{T}_0 \sim \tau N^2$ and dimensions $R^2 \sim Nb^2$ is,

$$D_0 \sim \frac{R^2}{\mathcal{T}_0} = \frac{Nb^2}{\tau N^2} = \frac{b^2}{\tau} \frac{1}{N} \tag{15}$$

For a sticky Rouse chain with $\rho_x \ll 1$, we can crudely approximate $\mathcal{T} \sim \tau_x N_x^2 + \tau N^2$ so that it is governed by the slowest (regular or sticky) Rouse mode. If the sticky modes dominate the late-time response, $\tau_x N_x^2 \gg \tau N^2$, then $\mathcal{T} \approx \tau_x N_x^2$, and,

$$D \sim \frac{R^2}{\mathcal{T}} = \frac{Nb^2}{\tau_x N_x^2} = \frac{b^2}{\tau_x}\frac{N}{N_x^2}. \tag{16}$$

Note that this argument implies $D \sim N_x^{-2}$, which is empirically observed for unentangled, lightly sulfonated polystyrene ionomers.[111] In general, however, the ratio of the diffusivities,

$$\frac{D_0}{D} = 1 + \frac{\tau_x N_x^2}{\tau N^2}. \tag{17}$$

For free-draining chains, we can obtain an expression for the ratio of the diffusivities in terms of the drag coefficient, using the Einstein relation. For a plain Rouse chain without any XLs, $D_0 = k_B T/(\zeta N)$, which is identical to eqn. 15 with $\zeta = k\tau$. For a sticky Rouse chain, the total drag may be written as $\zeta_x N_x + \zeta(N - N_x)$. The ratio of the diffusivities,

$$\frac{D_0}{D} = 1 + \frac{(\zeta_x - \zeta)N_x}{\zeta N}. \tag{18}$$

Comparing eqns 17 and 18, we find the ratio of the drag coefficients δ, corresponding to sticky and regular beads, is approximately proportional to the product of the τ_x and N_x,

$$\delta = \frac{\zeta_x}{\zeta} = 1 + \frac{\tau_x}{\tau}\frac{N_x}{N}. \tag{19}$$

When slow modes dominate the response, i.e., $\tau_x N_x \gg \tau N$, δ is proportional to the product of τ_x and N_x because $\delta \approx \tau_x N_x/(\tau N)$. As such, we obtain the anticipated $\zeta_x \sim \tau_x$ relation. In the opposite extreme, when the chain is lightly cross-linked ($\rho_x \ll 1$) and the lifetime of a XL is short ($\tau_x \sim \tau$), $\delta \approx 1$.

2.5 Temperature Dependence

The pre-exponential factor τ_x^0 in eqn 14 subsumes a lot of interesting and ill-understood physics. This is true even for interpreting chemical reaction experiments of non-polymeric systems. Over limited temperature windows, τ_x^0 is often assumed to be independent of temperature as its variability is typically dwarfed by the exponential term. However, this assumption of constancy can lead to serious errors (of the order of $\sim$10 - 50%) in estimating the activation energy from small molecule studies, especially when $E_a/RT \lesssim 10$.[112] When more precise analyses are required, especially when experiments are performed over a wide temperature range, τ_x^0 is modeled as a function of temperature. For polymers, a fundamental timescale is set by monomer friction. As such, it is perhaps natural to propose $\tau_x^0 \sim \tau$, where $\tau \sim \zeta/k$ is the elementary Rouse timescale. We set $\tau_x^0 = 2\tau$ to account for the decreased mobility of a XL bead which is connected to four strands, instead of two.[113] We discuss the repercussions of this assumption in sec. 4.1.

Above the glass transition temperature T_g, the temperature dependence of τ for polymers and networks is empirically described by the Williams-Landel-Ferry (WLF) equation,[114]

$$\log_{10} \alpha_T = \frac{-C_1(T - T_0)}{C_2 + (T - T_0)}, \tag{20}$$

where T_0 is the temperature at which $\alpha_T = 1$, and C_1 and C_2 are parameters. For $T \sim T_g$, α_T is usually very sensitive to temperature. However, at sufficiently high temperatures, where $T \gg T_\infty \equiv T_0 - C_2$, α_T becomes less sensitive to temperature. In this regime, the WLF equation can be described approximately using an Arrhenius form,[115]

$$\alpha_T \sim \exp\left(\frac{E_{\text{WLF}}}{RT}\right) \quad \text{with} \quad \frac{E_{\text{WLF}}}{RT} = \frac{2.303\, C_1 C_2 T}{(C_2 + T - T_0)^2}. \tag{21}$$

With this choice for τ_x^0, we anticipate acceleration of dynamics with increased temperature. Since τ_x is a product of a WLF and an Arrhenius term, its temperature dependence is stronger than both the WLF and Arrhenius contributions. This trend is indeed observed in ionomers, where

the formation and disassociation of XLs is governed by electrostatic interactions and dielectric contrast.[56] WLF parameters may be perturbed when chains are chemically modified to enable cross-linking; however, this perturbation is neglected in this work.

The modulus G_0 also varies with temperature, although it exhibits a somewhat weaker dependence. This change is often described using a vertical shift factor,

$$b_T = \frac{\rho(T)T}{\rho(T_r)T_r}, \tag{22}$$

where T_r is any convenient reference temperature. The WLF equation can be shifted to the reference temperature T_r, by defining,

$$a_T = \frac{\alpha_T(T)}{\alpha_T(T_r)}, \tag{23}$$

so that $a_T(T_r) = 1$, instead of the default $\alpha_T(T_0) = 1$.

3 Results

We first compare the IHR and SSR models to delineate the regime in which the latter is a useful approximation. We then probe the general properties of the IHR model, including the influence of XL distribution on viscoelasticity, which cannot be studied with the SSR model. We use the IHR model to study the temperature dependence of viscoelasticity for three different polymer matrices. We find that time-temperature superposition cannot be performed across the entire time spectrum using a single set of shift parameters. We finally investigate the temperature dependence of viscosity on the terminal relaxation time in these systems, and offer guidelines for ensuring accurate measurement of these parameters.

3.1 Comparison of IHR and SSR Models

Figure 2 compares the IHR and SSR models for different values of τ_x and N_x. We assume that $N = 119$, $\tau_b = \zeta/k = 1$, and that the XLs are distributed uniformly along the chain. As τ_x/τ

increases from 10^2 to 10^3, the "stickiness" of the XLs also increases. Regardless of this ratio, the correspondence between the IHR and SSR in the limit of $N_x = 0$ and $N_x = N$ is quite good. In these two limiting cases, only one of the two summations in eqn 10 describing the SSR model is operative. The response is effectively Rouse-like, which is evident in figure 2. The vertical dotted lines denote the Rouse relaxation times of the bare chain and fully sticky chain – τN^2 and $\tau_x N^2$, respectively. For the two limiting cases, $\delta = 1$ when $N_x = 0$, and $\delta \approx \tau_x/\tau$ (10^2 or 10^3) when $N_x = N$.

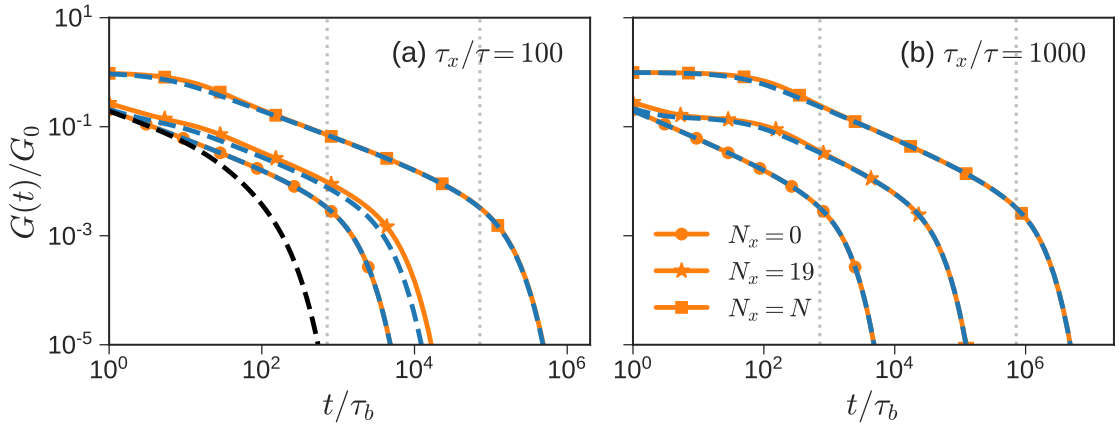

Figure 2: Comparison between SSR (dashed lines) and IHR (solid lines with symbols) models for a chain with $N = 119$ and varying values of N_x (marked by different symbols). The vertical dotted lines indicate the Rouse relaxation times of the bare chain ($N_x = 0$) and the fully sticky chain ($N_x = N$). For $N_x > \sqrt{\tau/\tau_x}N$, the correspondence between the two models improves, as the stickiness of the XLs increases. (a) τ/τ_x =100. The dashed black line shows the SSR response when $N_x = 4$, which is less than the critical threshold of $\sqrt{\tau/\tau_x}N$. (b) τ/τ_x =1000.

Figure 2 also illustrates the response for $N_x = 19$, where only some of the beads are sticky, rather than all or none. Its stress relaxation response lies between these two extremes. Values of N_x and N are chosen so that the number of beads between the uniformly spaced XLs is an integer. When $\tau_x/\tau = 10^3$ ($\delta \approx 160$), the agreement between the two models is still good because the sticky and regular Rouse modes are well-separated, i.e., $\tau_x N_x^2/\tau N^2 \approx 25$. In contrast, when $\tau_x/\tau = 10^2$ ($\delta \approx 16$), $\tau_x N_x^2/\tau N^2 \approx 2.5$, creating deviations between the two models that appear in figure 2a. In the case that the XL density is equal to or less than the critical limit $\rho_x = N_x/N \lesssim \sqrt{\tau/\tau_x}$,

violation of the $\tau_x N_x^2 \gg \tau N^2$ assumption causes the SSR model to fail. When $\tau_x/\tau = 10^2$, a value of $N_x < N/10 \approx 12$ generates a physically incorrect response. In figure 2a, for example, the dashed black line shows the response for $N_x = 4$. Despite the presence of sticky beads, this response decays *faster* than the bare Rouse chain.

Figure 3 plots the average relaxation time $\tau_\eta = \eta_0/G_0$, which more clearly demonstrates the failure of the SSR model. Here, τ_η is estimated using the IHR and SSR for $N = 119$ at $\tau_x/\tau = 10^1 - 10^3$ and as N_x is systematically increased. The $\tau_x/\tau = 10^2$ and 10^3 curves are shifted up by one and two decades, from $\tau_\eta^R/\tau_b \approx 10$ to ≈ 100 and ≈ 1000, respectively, to reduce visual clutter. At $N_x = 0$, both the IHR and SSR reduce to the bare Rouse chain, and the curves for all τ_x/τ values coincide at $\tau_\eta^R/\tau_b = N/12 \approx 10$ (see eqn 8). As N_x increases, the IHR predicts a monotonic increase in τ_η. Conversely, the SSR predicts an unphysical non-monotonic behavior. The τ_η obtained from the SSR decreases initially as N_x increases, reaches a minima, and then increases to catch up with the IHR result. This is most clearly visible at $\tau_x/\tau = 10^1$, but is present in all cases. As alluded to previously, this behavior is observed when the criterion $\tau_x N_x^2 \gg \tau N^2$ is violated; in this regime, the SSR is not expected to work.

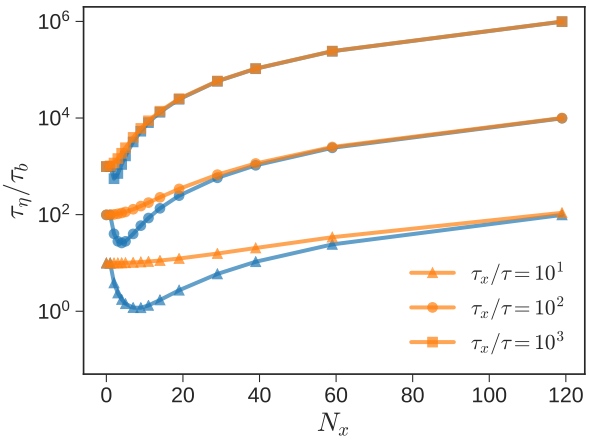

Figure 3: The characteristic relaxation time $\tau_\eta = \eta_0/G_0$ for the IHR (orange) and SSR (blue) models at $\tau_x/\tau = 10^1$ (triangles), 10^2 (circles), and 10^3 (squares) as a function of the number of XLs for a chain with $N = 119$ beads. XLs are distributed uniformly. The $\tau_x/\tau = 10^2$ and $\tau_x/\tau = 10^3$ curves are shifted upwards by a factor of 10 and 100, respectively, for improved visibility.

To summarize, when $\tau_x N_x^2 \gg \tau N^2$ and $N_x \gg 1$, the IHR and SSR models agree with each other. In this regime, it is perhaps preferable to use the SSR model due to its simplicity. This condition may be violated for chains with very few XLs (small N_x), or when the activation energy corresponding to the exchange reaction is relatively small. The latter is the case for dioxaborolane metathesis and imine exchange reactions, where $E_a^{\text{sm}} \approx 10 - 30$ kJ/mol was measured from small molecule analogues.[22] Under these circumstances, the use of the more general IHR model is advised. It has the advantage of being able to distinguish between different distributions of sticky beads, and remains valid even when τ_x and N_x are small.

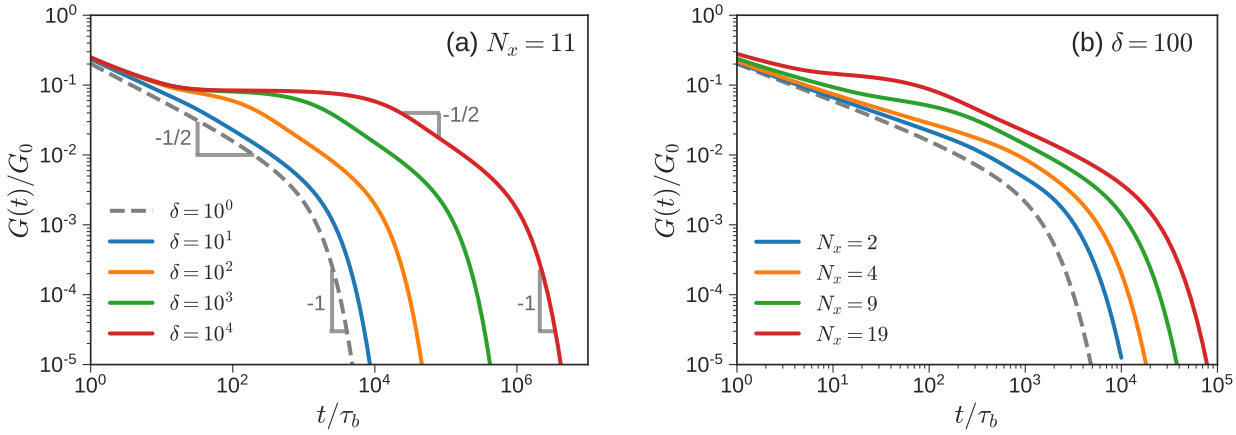

Figure 4: Normalized stress relaxation modulus for vitrimers with uniformly distributed XLs, as calculated by the IHR model. $G(t)$ is presented for varying (a) stickiness $\delta = \zeta_x/\zeta$ and (b) number of XLs N_x. Dashed line depicts the response of the bare Rouse chain with $N = 119$. For (a), relaxation dynamics are retarded as δ is increased. Slopes of -1/2 and -1 corresponding to the bare and sticky Rouse modes are identified. For (b), increasing N_x increases the terminal relaxation time and the plateau modulus.

3.2 Properties of IHR Model

Since the IHR model is both more general and robust than the SSR model, all results presented henceforth in this work are obtained from it. As our base case, we consider once again a chain with a total of $N = 119$ monomers. XLs are uniformly distributed along the backbone, and values of N_x are chosen so that the spacing between XLs is an integer. This choice ensures that the IHR model

calculations are not jagged, and are free from artifacts that arise due to rounding or truncation.

Figure 4a portrays the change in $G(t)$ as the stickiness of the beads $\delta = \zeta_x/\zeta$ is increased from 1 to 10^4. Here, $N_x = 11$ so that $\Delta N = 10$. The dashed gray line represents the case where $\delta = 1$ and $\zeta_x = \zeta$, which is equivalent to the response of the bare Rouse chain. When δ is increased to 10, the dynamics of the chain are retarded, and the $G(t)$ curve shifts rightward. As δ is increased further the response becomes slower. For $\delta > 1$, the initial decrease in the modulus deviates from the $G(t) \sim t^{-1/2}$ trend of the bare Rouse chain. For sufficiently large $\delta \sim 10^3 - 10^4$, the plateau associated with the XLs becomes conspicuous. The height of this plateau $G_x = \rho_x G_0$ is independent of δ. The terminal relaxation associated with XL exchange reactions also follows a Rouse-like pattern; beyond the plateau, we observe a second characteristic $G(t) \sim t^{-1/2}$ regime, before complete relaxation at approximately $\tau_x N_x^2$. For large δ and fixed $\rho_x = N_x/N$, eqn 19 implies that τ_x is proportional to δ. In this regime ($\delta \gtrsim 10^2$), the average relaxation time $\tau_\eta \sim \delta$. As δ increases by a factor of 10, τ_η and η_0 also increase by a factor of 10.

Figure 4b depicts the variation of the modulus with the number of XLs. As in figure 4a, we consider a chain with $N = 119$ and uniformly distributed XLs. Here $\delta = 100$ is held fixed. The dashed line corresponding to the bare Rouse chain is indeed the same in both subfigures. As N_x increases from 2 to 19, the number of monomers between successive XLs falls from 40 to 6. Unlike δ, increasing N_x affects both G_x and τ_η. G_x increases with increasing N_x because it is proportional to ρ_x. τ_η increases with the number of XLs, becoming approximately proportional $\tau_\eta \sim N_x$ for $N_x \gg 1$. This can be understood through the standard Rouse model dependence of viscosity on molecular weight, or eqn 8, where N and τ_b are replaced by the number of sticky Rouse beads N_x and their lifetime τ_x, respectively.

Figure 5 focuses on the effect of the XL distribution. In figure 5a, we consider uniform and random distributions for a chain with $N_x = 4$, 14, and 29 XLs. For the random distribution, we report an average over 1000 independent replicas. At a given value of N_x, the stress response of the two distributions is effectively the same. Unlike the IHR, the SSR model cannot directly account for the impact of the distribution of the XLs on the dynamics. However, in the large N_x regime

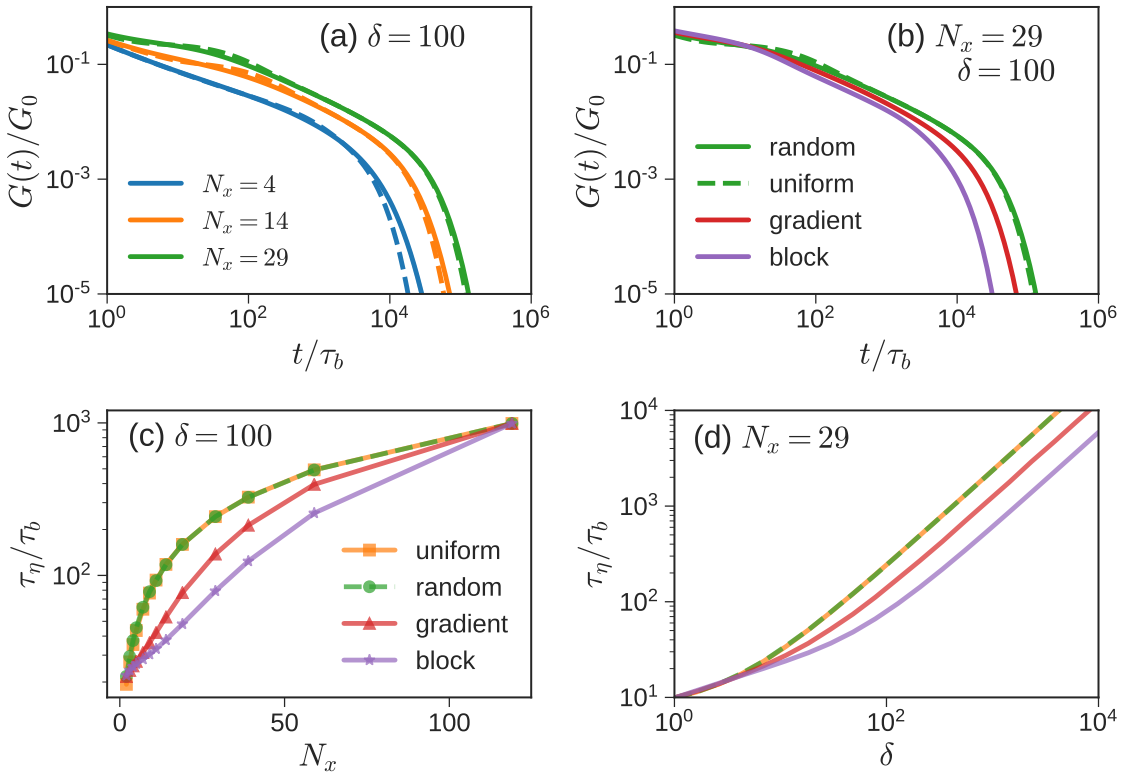

Figure 5: (a) Solid and dashed lines depict the stress relaxation response for randomly and uniformly distributed XLs, respectively, for a chain with $N = 119$ and $\delta = 100$. Three different values of $N_x = 4$, 14, and 29 are shown. Subfigure (b) focuses on one of these samples ($N_x = 29$), and compares the response of uniform and random XL distributions with blocky, and gradient distributions. The average relaxation time τ_η (proportional to η_0) is plotted as a function of (c) N_x with δ = 100, and (d) δ with N_x = 29.

the insensitivity to random or uniform distribution suggests that the SSR is a reasonable model to compute the linear viscoelasticity of random or uniformly distributed XLs.

Figure 5b concentrates on $N_x = 29$, and compares the response of the gradient and block distributions to the uniform and random distributions shown previously. Due to its stochastic nature, the response of the gradient distribution is averaged over 1000 independent replicas, just like random distribution. It shows significantly faster relaxation than random or uniform distributions. This is further exaggerated for block distributions, in which sticky beads are completely sequestered to one of the chain ends. Qualitatively, these observations are general, and persist for a broad range of values of N, N_x, and δ.

Figure 5c examines the average relaxation time τ_η as a function of distribution type. We consider chains with $N = 119$ and $\delta = 100$, and vary the number of XLs/chain. As expected, τ_η is independent of distribution type for the extreme cases of $N_x = 0$ (bare Rouse chain) and $N_x = N$ (all beads are sticky). The difference between random and uniform distributions is barely perceptible over the entire range of N_x explored. The gradient and block distributions follow trends that are anticipated from figure 5b. At a given N_x, as the distribution of XLs changes from even or approximately even (uniform/random) to concentrated at one of the ends approximately (gradient) or strictly (block), η_0 decreases.

Figure 5d varies δ between $10^0 - 10^4$, with $N_x = 29$ held constant. For sufficiently large δ ($\gtrsim 500$), $\tau_\eta \sim \delta$ is independent of the type of distribution. However, the relative order of viscosities (uniform $\approx$ random $>$ gradient $>$ block) is preserved. In this limit, the ratio of viscosities with different distributions becomes constant. At the other end, as δ approaches 1 and the sticky beads become less sticky, the four curves converge to the bare Rouse chain result.

To summarize, the IHR model can explore the linear viscoelastic response as a function of XL distribution. The linear rheology of uniform and random distributions of XLs are similar, and converge in the limit of large N_x. For uniformly distributed XLs, when $\delta \gtrsim 500$ and $N_x \gtrsim 20$ the IHR model predicts that the average relaxation time τ_η is approximately proportional to δ and N_x.

The plateau associated with XLs, G_x, is independent of δ but proportional to N_x. At a given value of δ and N_x, the relative order of viscosities η_0 for different XL distributions is given by uniform $\approx$ random $>$ gradient $>$ block. This trend, however, is only applicable for homogeneous vitrimer systems where χ-parameter between regular and sticky beads is zero.

Table 1: Selected properties of three common vitrimer matrices: polydimethylsiloxane (PDMS), polystyrene (PS), and poly(methyl methacrylate) (PMMA).

	PDMS	**PS**	**PMMA**
N_e	165	127	100
M_e	12293	13309	10013
T_g [K]	150	373	407
WLF parameters[115,116]			
C_1	1.9	12.7	9.4
C_2 [K]	222	50	447
T_0 [K]	303	373	463

3.3 Temperature Dependence of Viscosity

We now use the IHR model to examine the thermorheological properties of model vitrimers. Table 1 shows the properties of vitrimer matrices based on polydimethylsiloxane (PDMS), polystyrene (PS), or poly(methyl methacrylate) (PMMA).[115,116] As a base case, we first consider PDMS with $N = N_e$ and $N_x = 10$ uniformly spaced XLs. We set $E_a^{\text{sm}} = 28.1$ kJ/mol, corresponding to the measured activation energy of metathesis between small molecule dioxaborolanes.[22] Since G_0 and τ_b are also functions of temperature, we select a reference temperature $T_r = 413$ K, and express the modulus and time by normalizing with $G_0^r = G_0(T_r) = \rho R T_r / M_0$ and $\tau_b^r = \tau_b(T_r)$, respectively. To decouple the temperature dependence of the XL exchange kinetics and monomer friction, we define an Arrhenius shift factor (e_T) that is analogous to the WLF shift factor (a_T, eqn. 20),

$$\log e_T = \frac{E_a^{\text{sm}}}{R}\left(\frac{1}{T} - \frac{1}{T_r}\right). \tag{24}$$

Figure 6a shows the acceleration in the PDMS vitrimer dynamics as temperature is increased.

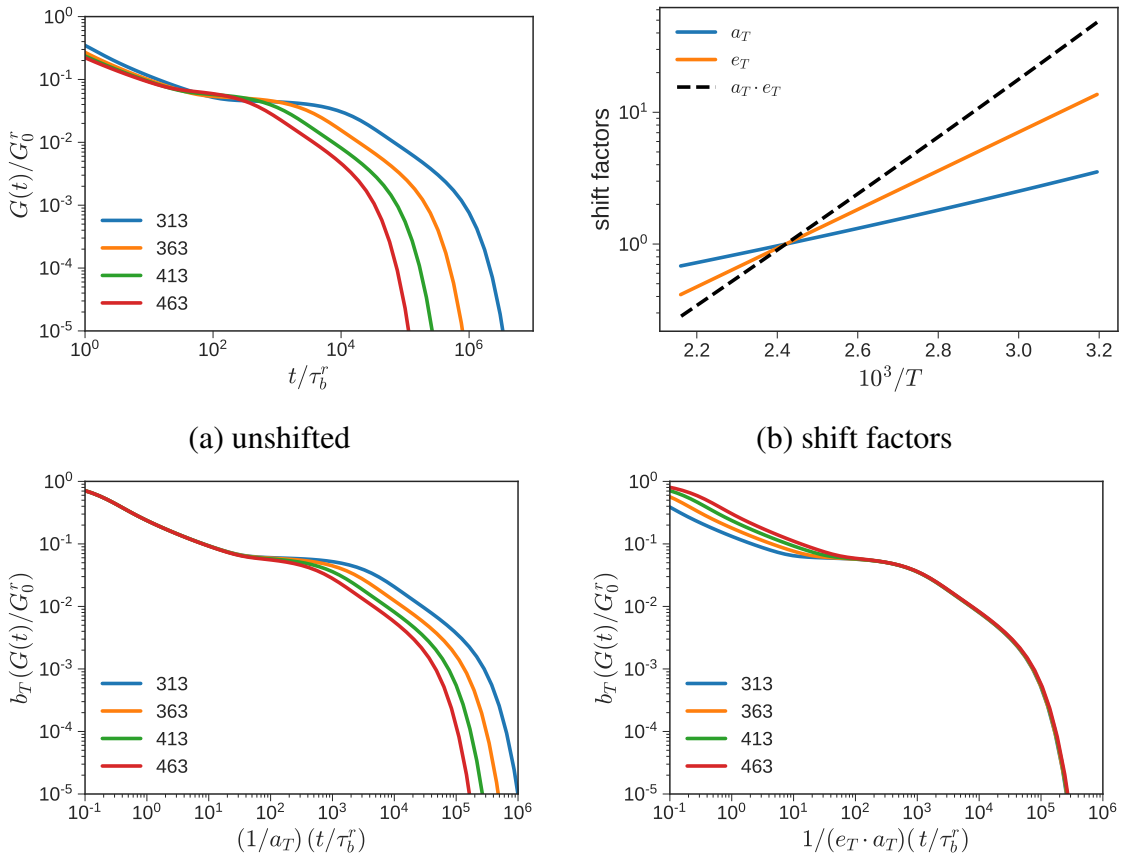

(a) unshifted

(b) shift factors

(c) WLF shift

(d) WLF-Arrhenius shift

Figure 6: (a) Stress relaxation of PDMS with $N = N_e$ and $N_x = 10$ XLs uniformly distributed along the chain as temperature is varied between 313–463 K. (b) The WLF and Arrhenius temperature shift factors. The response from (a) is shifted vertically, and horizontally using (c) WLF and (d) combined WLF-Arrhenius shift factors.

For context, as T increases from 313–463 K, δ falls about 30$\times$ from $\sim$6000 to $\sim$180 (see figure S1), while $G_0 \sim T$. Thus, the change in the modulus is much weaker; it increases only by 50%, even over this artificially large window of temperature spanning 150 K. On a log-log plot, this change is not clearly visible. Because the effect of temperature is manifested primarily through variation in δ, figure 6 bears a qualitative resemblance to figure 4a. The plateau due to the XLs has a modulus that is insensitive to δ, and is followed by Rouse-like relaxation.

Figure 6b plots a_T and e_T for this system as a function of inverse temperature for $T = 313$ – 463 K. They intersect at $T_r = 413$ K, where both a_T and e_T are equal to unity by definition. For PDMS, this temperature range is sufficiently removed from the glass transition temperature and $T_\infty = T_0 - C_2 = 81$ K. Consequently, the WLF equation takes the approximate Arrhenius form given by eqn 21, which is evident from the linear dependence of $\log\, a_T$ on $1/T$ in the subfigure. For PDMS, the dependence of a_T on temperature is weaker than the e_T dependence, largely due to the small value for the coefficient C_1. As shown shortly, this is atypical; PS and PMMA, for example, have relatively high T_∞ and C_1. If $\tau_x^0 = 2\tau$, as assumed here, the overall dynamics are governed by τ_x through a product of a_T (monomer friction) and e_T (XL exchange).[117] This is shown by the dashed black line in figure 6b. This dependence is stronger than either a_T or e_T. Activation energies inferred from the slopes of a_T, e_T, and the product $a_T \cdot e_T$, are 11.5, 28.1, and 39.6 kJ/mol, respectively.

Figures 6c and 6d apply the horizontal and vertical shift factors to the PDMS vitrimer stress relaxation data. b_T, a_T, and e_T are calculated using eqns 22, 23, and 24. Since the temperature dependence of monomer friction and XL dynamics are different, time-temperature superposition (TTS) cannot be performed using a single set of horizontal shift factors. When the curves are shifted using the WLF shift factor a_T (figure 6c), only the short time dynamics superimpose ($t \lesssim \tau_x^0$). When the curves are shifted using the combined WLF-Arrhenius shift factor e_T (figure 6d), the long time dynamics collapse ($t \gtrsim \tau_x^0$). Concurrently, there is a dispersion at short times. This divergence in superposition suggests that the short and long time dynamics are governed by different processes. The short time dynamics are controlled by the mobility of the monomer, as

specified by the WLF equation $\tau(T)/\tau(T_r) = a_T$, where $\tau(T_r)$ is the elementary Rouse timescale at the reference temperature. In this regime, the network is unaware of XL exchanges. The long time dynamics, however, are dictated by the combination of network strand relaxation and XL exchange. Mathematically, this implies that the longest relaxation time of the IHR model obeys the relationship $\tau_1(T)/\tau_1(T_r) \approx a_T \cdot e_T$.

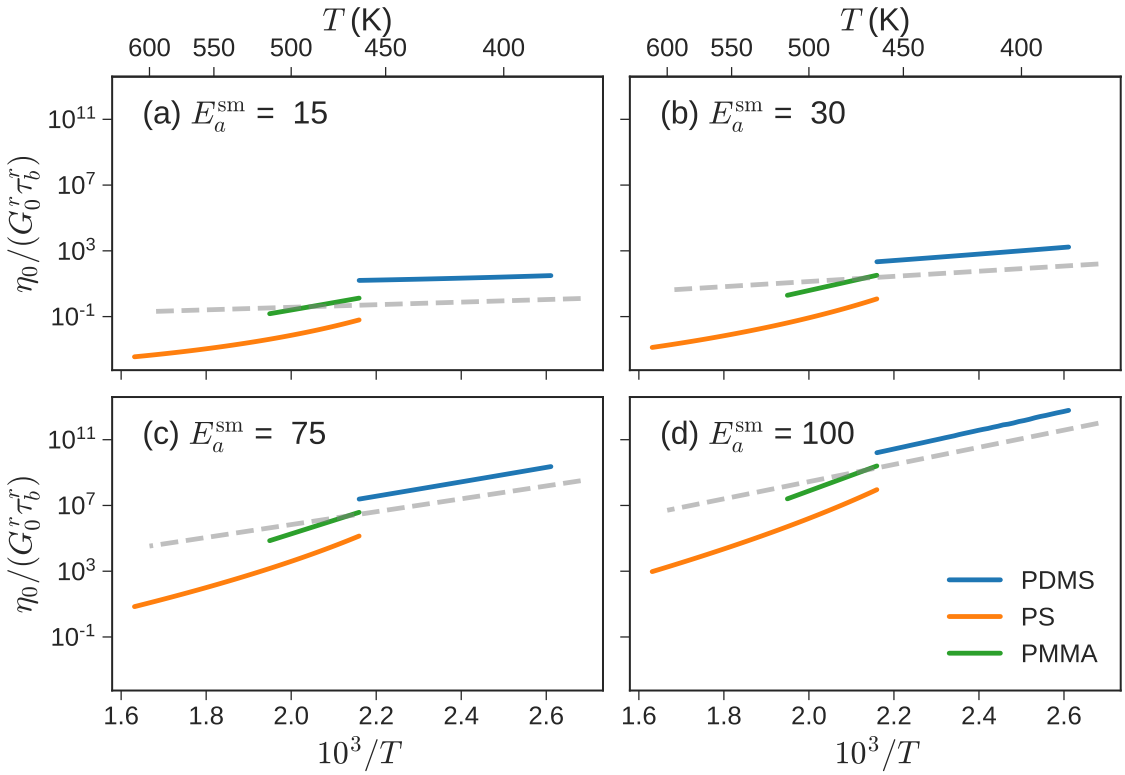

Figure 7: Solid lines depict viscosity as a function of inverse temperature of PDMS (blue), PS (orange) and PMMA (green) using $\tau_x^0 \sim \tau$. The slope of the dashed lines is proportional to the small molecule exchange reaction activation energies $E_a^{\mathrm{sm}} = 15, 30, 75$ and 100 kJ/mol, as indicated on the subplots.

Figure 7 depicts the variation in η_0 as a function of inverse temperature for PDMS, PS, and PMMA vitrimers that have $N = N_e$ and $N_x = 10$ uniformly spaced XLs. η_0 is normalized by the product of G_0 and the monomer relaxation time at the reference temperature (which has units of viscosity). We neglect the change in polymer density, and assume $G_0 \sim T$. In the figure, the temperature ranges used for PDMS, PS, and PMMA are 383–463 K, 463–613 K, and 463–

513 K, respectively. The four subplots span the spectrum of activation energies that have been observed for various vitrimer XL chemistries. $E_a^{\text{sm}} = 15$ and 30 kJ/mol correspond to the lower and upper limits for small molecule dioxaborolane and imine metathesis.[22] $E_a^{\text{sm}} = 75$ kJ/mol and 100 kJ/mol are consistent with transesterification.[67] The range of the inverse temperature and normalized viscosity in the four subplots is kept identical to illustrate both the change in magnitude, and the slope as a function of E_a^{sm}. By comparing each subplot, we observe that the viscosity changes by several orders of magnitude as the activation energy increases. This is expected because viscosity is governed by the XL exchange reactions which slow down exponentially with increasing E_a^{sm}.

Figure 7 also highlights the different temperature responses for each vitrimer matrix. PDMS vitrimer exhibits the classical Arrhenius-type dependence $\log \eta_0 \sim 1/T$. This is related to figure 6b; at sufficiently high temperatures, WLF follows an apparent exponential form. The slope of η_0 versus $1/T$ gives the activation energy from viscosity, E_a^{rh}. In nearly all cases, $E_a^{\text{rh}} > E_a^{\text{sm}}$. This indicates that, in general, the activation energy inferred from rheology is larger than the activation energy obtained from small molecule studies. In contrast to PDMS, PS vitrimer exhibits curvature for η_0 versus $1/T$, especially at low temperatures (high $1/T$) (see figure S2). At low temperatures, WLF contributions are manifested by nonlinearity in the η_0 versus $1/T$ plot. At sufficiently high temperatures, however, the non-Arrhenius behavior that arises from WLF modes can be visually masked over a limited temperature range. PMMA vitrimer demonstrates an apparent Arrhenius-type dependence for η_0 due to the limited temperature range that is explored.

Figure 8 compares E_a^{rh} obtained from the figure 7 against the underlying E_a^{sm}. E_a^{rh} is extracted from the high temperature (low $1/T$) part of the temperature window, where Arrhenius-type dependence is observed. The smallest discrepancy between E_a^{rh} and E_a^{sm} is observed for PDMS, where the two energies deviate by about 15%. This is consistent with the reasonably close correspondence between the slopes of the PDMS η_0 curves and the E_a^{sm} dashed lines in figure 7. E_a^{rh} increases from ≈12 kJ/mol to 109 kJ/mol as E_a^{sm} increases from 15 to 100 kJ/mol. The difference between E_a^{rh} and E_a^{sm} is larger for PS and PMMA. For activation energies of 30 kJ/mol and

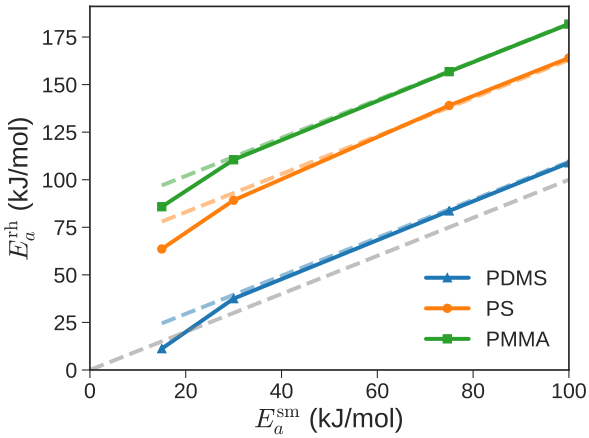

Figure 8: E_a^{rh} versus E_a^{sm} for the cases considered in figure 7. The dashed gray line is the dependence expected for $E_a^{\mathrm{rh}} = E_a^{\mathrm{sm}}$. Dashed blue, orange, and green lines denote E_a^{sm} offset by 10, 63, and 82 kJ/mol, respectively. These offsets are approximately equal to E_{WLF} corresponding to the three polymers.

above, the difference $E_a^{\mathrm{rh}} - E_a^{\mathrm{sm}} \approx E_{\mathrm{WLF}}$ is approximately constant and is equal to about 10 kJ/mol for PDMS, 65 kJ/mol for PS, and 80 kJ/mol for PMMA. In this regime, a simple approximate relationship between the two activation energies exists, and is given by $E_a^{\mathrm{rh}} \approx E_a^{\mathrm{sm}} + E_{\mathrm{WLF}}$.

This is not surprising; indeed it is a manifestation of the observation that terminal relaxation at different temperatures can be superposed by using the combined WLF-Arrhenius shift factors (see figure 6d, for example). For temperatures sufficiently above T_g, a_T approximately follows an Arrhenius relationship, as does the product $a_T \cdot e_T$ (see figure 6b). Note that deviations from $E_a^{\mathrm{rh}} = E_a^{\mathrm{sm}} + E_{\mathrm{WLF}}$ are expected when $T \sim T_g$, as a_T does not follow an Arrhenius form at that temperature regime.

To summarize, the IHR model predicts that the vitrimer matrix and XL chemistry profoundly impact viscoelasticity. For all samples, the short time dynamics are controlled by monomer friction, while the long time dynamics are governed by the combination of network strand relaxation and XL exchange. The viscosity of PDMS vitrimers, which have a fairly low T_g, demonstrates the expected Arrhenius temperature dependence. For PS vitrimers, which have high T_g, Arrhenius behavior is only displayed at very high temperatures. PMMA vitrimers exhibit Arrhenius behav-

ior over the small temperature range that was explored. For temperatures sufficiently above T_g, the observed E_a^{rh} for all systems can be estimated a priori using the E_a^{sm} and WLF parameters, as $E_a^{\text{rh}} \approx E_a^{\text{sm}} + E_{\text{WLF}}$, where E_{WLF} is given by eqn 21. This explains the general observation $E_a^{\text{rh}} > E_a^{\text{sm}}$.

4 Discussion

4.1 Influence of Pre-exponential Factor on Temperature Dependence

For the generalized sticky Rouse model approach presented in this manuscript, the drag on a sticky bead is proportional to $\tau_x = \tau_x^0 e^{E_a^{\text{sm}}/RT}$, where the pre-exponential factor $\tau_x^0 = \sigma\tau$. We treated σ as a constant, i.e., $\sigma = 2$. While the functional form of τ_x^0 is simple, it relies on two major assumptions: (i) σ is independent of temperature and cross-link density, and (ii) the monomer relaxation time τ follows a WLF relationship with temperature.

The assumption of independence of σ with temperature is consistent with established theoretical models of XL dynamics,[113] but it neglects the elaborate choreography involved in bringing two XLs together to facilitate an exchange reaction. Associative cross-linking within a vitrimer is not a mean-field process; the density, spatial distribution and orientation of the cross-links most likely play an important role. As proposed by de Gennes, reactive groups attached to flexible polymer chains explore their surroundings via sub-diffusive and compact random walks.[118] Based on this idea, the tethering of the vitrimer XLs to network strands reduces their mobility and probability of encountering another XL, reactive group, or catalyst.[113,119,120] XLs may even reassociate with old partners in ways that do not relieve stress along the backbone.[84] These impediments significantly delay terminal relaxation by orders of magnitude.[121] Although the influence of vitrimer structure on XL mobility is outside the scope of this study, it can potentially be evaluated through the IHR or SSR models by treating σ as a fitting parameter rather than a constant. Precise calculation of σ will permit accurate estimation of processing parameters, e.g., η_0 and T_v. However, we must emphasize that like the standard Rouse model, the IHR is fundamentally a single chain model. It

cannot directly account for nontrivial multi-chain interactions.

The WLF assumption, standard for polymeric systems, establishes the combined temperature dependence of τ and the exponential factor. Consequently, E_a^{rh} is predicted to be greater than E_a^{sm} for PDMS, PMMA, and PS vitrimers. The difference between two activation energies is approximately equal to E_{WLF}, especially for $T \gg T_g$. For PDMS, $E_{\text{WLF}} \approx 10$ kJ/mol, the difference between the two activation energies is within experimental uncertainty. For PMMA and PS, E_{WLF} is approximately equal to 65 kJ/mol and 80 kJ/mol, respectively, making it greater than E_a^{sm} in some cases. This relationship among E_a^{rh}, E_a^{sm}, and E_{WLF} provides a simple and convenient method for predicting viscosity. However, the mechanism of the XL exchange within the vitrimer matrix will impact the relationship between E_a^{rh} and E_a^{sm}. If another process that has a weaker temperature dependence is rate-controlling, e.g., proper alignment of reacting elements, then $\tau_x^0 \sim \tau$ may no longer be valid. In such a situation, σ would dominate τ_x^0. Small molecule diffusion, which typically has an Arrhenius temperature dependence,[56] may also mediate XL exchange in externally catalyzed vitrimers. If catalyst transport is the rate limiting step for relaxation, then τ_x^0 inherits the Arrhenius relationship. A plot of $\log \eta_0$ versus $1/T$ would be linear, but the slope of the line would be a function of the activation energy for catalyst diffusion.

4.2 Recommended Practices to Extract Accurate $\mathbf{E_a^{rh}}$

Conceptually, vitrimers are viscoelastic liquids. At sufficiently high temperatures and long timescales they reach terminal relaxation, and their relaxation corresponds to a unique zero-shear viscosity η_0. As mentioned previously, τ_η and η_0 depend on the slowest relaxation mode, τ_1. Thus, timespans of $t > \tau_1$ *need* to be evaluated to accurately probe these parameters. Otherwise, the estimated τ_η and η_0 are not unique, and are influenced by the method of both measurement and analysis.

Figure 9 depicts simulated vitrimer linear viscoelasticity data for various types of rheology experiments: stress relaxation, creep, and small amplitude oscillatory shear. To find η_0, one must first check if the sample has indeed completely relaxed by looking for a characteristic rheological

signature. Depending on the experiment used, this is manifested in different ways. For stress relaxation, $\log G(t) \sim t$; for creep compliance, $J(t) \sim t$; for small amplitude oscillatory shear, $G'(\omega) \sim \omega^2$ and $G''(\omega) \sim \omega$. Caution must be exercised in interpreting η_0 obtained when these signatures of terminal relaxation cannot be ascertained.

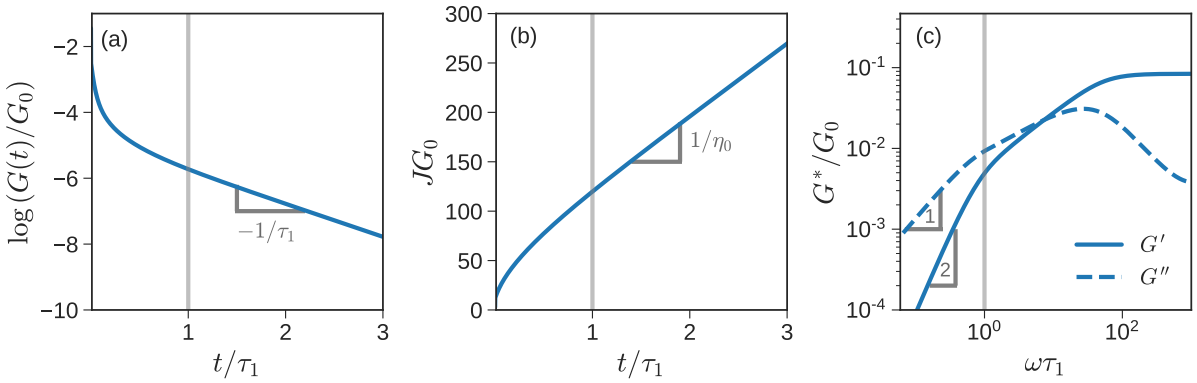

Figure 9: Normalized (a) $G(t)$, (b) $J(t)$, and (c) $G^*(\omega)$ are replotted for the $\delta = 10^4$ sample considered in figure 4(a) to highlight signs of terminal relaxation. The horizontal time or frequency axis is normalized by the longest relaxation time τ_1, which is also marked using a vertical gray line. For $t > \tau_1$ and $\omega < 1/\tau_1$, signatures of terminal relaxation are observed, viz. $\log G(t) \sim -t/\tau_1$, $J(t) \sim t/\eta_0$, and $G' \sim \omega^2$ and $G'' \sim \omega$.

Figure 9a depicts the $G(t)$, $J(t)$, and $G^*(\omega)$ for the $\delta = 10^4$ sample previously considered in figure 4a, where $G(t)$ was shown on a log-log plot. To convert $G(t)$ to $J(t)$ in figure 9b we used the spectrum of relaxation times $\{\tau_i\}$ obtained from the IHR model, and performed interconversion to creep compliance using the Prony series method.[122,123] As evident from figure 9, we need to probe times of the order of $2-5\tau_1$ to ascertain characteristic signatures of terminal relaxation associated with these measurements.

Although accurate evaluation of E_a^{rh} requires the sample to reach terminal relaxation, rheological measurements on vitrimer systems have been typically run for inadequate timespans. Failure to reach $t \gtrsim \tau_1$ can create systematic errors in the estimation of E_a^{rh}. To emphasize this point with a concrete example, we reconsider the PDMS sample used in figure 6a. Recall that for this sample, $N = N_e$, $N_x = 10$ (uniformly dispersed XLs), and $E_a^{\text{sm}} = 28.1$ kJ/mol.

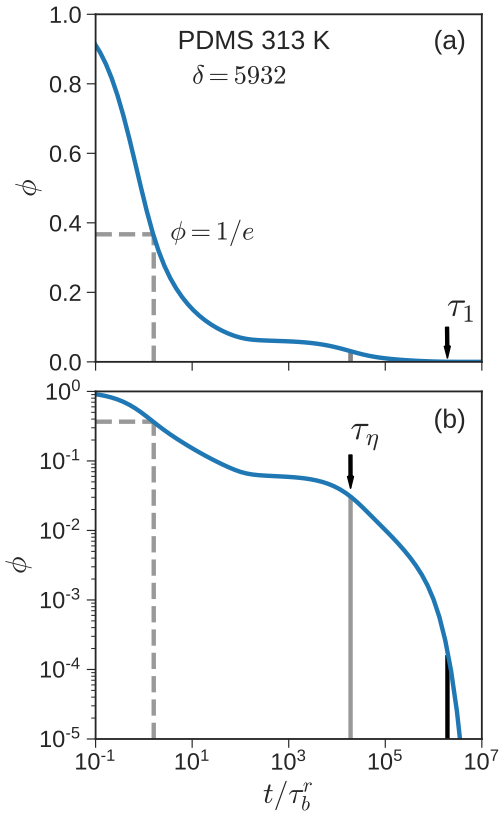

Figure 10: Normalized stress relaxation modulus for PDMS at 313 K plotted on (a) linear and (b) logarithmic scales. The location where $\phi(t)$ falls to $1/e$ of its initial value is indicated by dashed lines. Locations of the longest and average relaxation times τ_1 and τ_η are indicated by arrows in (a) and (b), respectively.

Figure 10 plots the normalized stress relaxation function $\phi(t)$ at a particular temperature, viz. the $T = 313$ K sample, with linear and logarithmic vertical axes. The horizontal axis is common and logarithmic. A popular, but ill-advised, procedure for determining the characteristic relaxation time τ^* from stress relaxation experiments is to define it as the time point where $\phi(t)$ falls to $1/e$ of its original value (marked by dashed gray lines in the figure). Fundamentally, this threshold is appropriate if relaxation is governed by a single Maxwell mode (in which case, $\tau^* = \tau_1 = \tau_\eta$). For polymeric systems with a wide spectrum of relaxation times, however, this is inaccurate. In particular, for vitrimer systems this method runs the risk of probing timescales much shorter than τ_x^0, and underestimating η_0 by several orders of magnitude. As shown in the figure, the difference between these characteristic timescales defined as either $\phi(\tau^*) = 1/e$ or as the longest relaxation time $\tau^* = \tau_1$ (marked in black), is over five decades. More problematically, using the $1/e$ threshold complicates the analysis of the temperature dependence of τ^*. As observed in figure 6, TTS cannot be obtained using a single set of parameters. Any estimates of τ^* obtained by probing $t < \tau_x^0$ only reveal the influence of temperature on the elementary Rouse timescale τ (and perhaps τ_x^0), but not τ_x or τ_1.

Figure 11 shows how the method used to specify the characteristic relaxation time τ^* impacts the estimated activation energy E_a^{rh}. Since E_a^{rh} is obtained from the slope of $\log \tau^*$ versus $1/T$, the (logarithmic) vertical axis is normalized by τ^* at the reference temperature $T_r = 413$ K (τ_r^*), which causes different curves to pass through a common point. When τ^* is defined through $\phi(\tau^*) = 1/e$ (blue), the activation energy estimated from the slope is comparable with $E_{\text{WLF}} \approx 11$ kJ/mol which is shown by the dashed line. This is not surprising, since $1/e \approx 0.37$ is greater than the $G_x/G(0) \approx 0.1$ plateau in fig 10 which is associated with the XLs. Thus, τ^* determined using this criterion effectively probes the temperature dependence of short time dynamics, i.e., chain friction. On the other hand, the E_a^{rh} estimated when τ^* is defined as either the average (τ_η) or longest relaxation time (τ_1) are identical. It corresponds quite well with the activation energy estimated using $E_a^{\text{rh}} = E_a^{\text{sm}} + E_{\text{WLF}} \approx 40$ kJ/mol, shown by the dotted line.

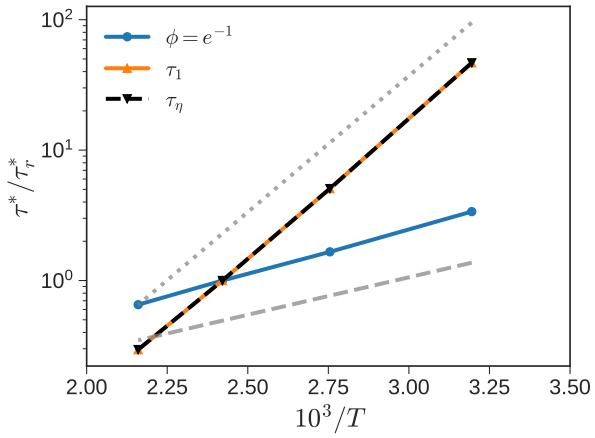

Figure 11: Arrhenius plot of the characteristic relaxation time τ^*, determined using three different methods, versus inverse temperature for the PDMS samples shown in figure 6a. τ^* is normalized by the characteristic relaxation time at $T_r = 413$ K (τ_r^*) to facilitate comparison of slopes. The overlapping orange and dashed black lines correspond to τ_1 and τ_η respectively. Blue circles denote τ^* obtained using $\phi(\tau^*) = 1/e$. The slopes of the dashed and dotted gray lines correspond to $E_{\text{WLF}} \approx 11$ kJ/mol, and $E_a^{\text{rh}} = E_a^{\text{sm}} + E_{\text{WLF}} \approx 40$ kJ/mol, respectively.

4.3 Utility and Limitations of IHR and SSR Models for Vitrimer Systems

The IHR and SSR models are powerful tools for forecasting and analyzing vitrimer viscoelasticity. They capture many of the rheological signatures that have been observed experimentally (e.g., Arrhenius temperature dependence, secondary peaks and plateaus in small amplitude oscillatory shear, strong dependence on the matrix and XL chemistry). Based only on knowledge of the vitrimer composition and XL exchange kinetics, they predict the linear viscoelastic response across the entire time/frequency domain for multiple types of measurement techniques. To achieve a specific rheological profile, the optimal pairing of XL structure and backbone can be identified a priori. Moreover, these models offer insight into the network topology and dynamics. The presence of defects in the vitrimer network may be probed by comparing the measured plateau modulus G_0 to the anticipated value from rubber elasticity theory.[124–127] σ potentially serves as a proxy for XL mobility, as mentioned earlier. Thus, the IHR and SSR can serve as platforms for connecting macroscopic flow behavior (as determined by rheology) to microscopic dynamics (as observed by dielectric relaxation spectroscopy or other techniques).

While these models can be used to advance understanding of structure-property relationships, they do have limitations. Generalized Rouse models like the IHR or SSR only apply to homogeneous vitrimers composed of unentangled linear chains; the XLs solely interact with the backbone monomers via the propagation of frictional drag. In real vitrimers, however, branches and entanglements enhance the elasticity and delay relaxation.[43–46] Strong thermodynamic interactions between the XLs and backbone induce concentration fluctuations and macro/microphase separation.[12,13,47–49] Slip link models have the capability to resolve multi-chain interactions in entangled polymer melts, and early work shows much promise.[73] They are sufficiently coarse-grained to access long relaxation times observed at low temperatures, while retaining the ability to model the complex interchain dynamics.[128–130] Furthermore, as seen from the comparison of the SSR and IHR models, if the timescales associated with chain relaxation and kinetics of exchange reactions are well-separated, we can envision a hierarchy of additive models, ranging from molecular dynamics that capture fine details of chain motion to slip link models that resolve terminal relaxation.

In this work, we identify the conditions under which vitrimer viscosity follows an Arrhenius temperature dependence. Yet, vitrimers are not unique in this regard. Many types of polymeric systems have Arrhenius rheology.[131–134] In particular, polymer networks with dissociative covalent XLs express this relationship because their network connectivity hinges on the equilibrium balance between the bonded/debonded states of the XLs.[3] This mechanism is identical to that of the dynamic polymer networks outlined in the original sticky Rouse and sticky reptation papers.[82–85] As such, the IHR and SSR models presented here can be adapted for systems with dissociative covalent XLs, but the XL density N_x must be modified so that it is a function of temperature.

The similarity in rheological behavior, however, does not mean vitrimers and dissociative covalent polymer networks are the same. Vitrimer XLs maintain network connectivity at all temperatures, rendering them insoluble in good solvents. In contrast, dissociative covalent polymer networks will dissolve. Vitrimers are unique among polymers because of their combination of insolubility and processability. Both properties are necessary criteria for determining if a material is a vitrimer. It is not sufficient to only characterize their rheology.

5 Conclusions

Using the IHR model for unentangled, fully developed vitrimer networks, we find that the temperature dependence of the rheology is a product of WLF and Arrhenius contributions. Consequently, the effective activation energy determined from rheology, E_a^{rh}, is typically larger than the activation energy for the exchange reaction between small molecule analogues, E_a^{sm}. The difference between E_a^{rh} and E_a^{sm} depends strongly on the chemistry of the polymer matrix and the temperature range investigated, even when the XL chemistry is the same. At sufficiently high temperatures, $E_a^{\text{rh}} \approx E_a^{\text{sm}} + E_{\text{WLF}}$. For PDMS vitrimer, E_{WLF} is relatively small, and $E_a^{\text{rh}} \approx E_a^{\text{sm}}$. On the other hand, for PMMA vitrimers, $E_{\text{WLF}} \approx 80$ kJ/mol is large, resulting in substantial differences between E_a^{rh} and E_a^{sm}. Similar trends are observed for PS vitrimers; however, at the lower end of the temperatures probed, non-Arrhenius behavior is observed. Estimation of E_a^{rh} from an Arrhenius plot depends on the determination of η_0 or τ^*. Systematic errors that arise from some common but ill-advised methods of data analysis are illustrated using the IHR model.

As a consequence of WLF and Arrhenius contributions, time-temperature superposition cannot be achieved over the entire relaxation spectrum. Use of WLF shift factors allows superposition of short time dynamics, which corresponds to relaxation of individual monomers. In contrast, a combination of WLF and Arrhenius shift factors are required to obtain superposition of long time relaxations due to the interplay between backbone relaxations and XL exchanges. This is similar to observations in other dynamic polymer network systems.

A comparison of the SSR and IHR model indicates that the SSR is a good approximation when three conditions are met: (i) $N_x \gg 1$, (ii) $\tau_x N_x^2 \gg \tau N^2$, so that the sticky modes are well-separated from the regular Rouse modes, and (iii) the distribution of XLs is random or uniform. However, when any of these conditions is violated, use of the IHR model is advised. The rheology of a sticky Rouse model with random and uniformly distributed sticky beads are expected to be within experimental error limits, especially as N_x increases. However, gradient and block distributions are quite different, and typically relax much faster than random and uniform distributions.

Vitrimers are a unique class of polymers, and there is still much left to be learned about their flow behavior. The first decade of vitrimer research has enabled the preparation of well-defined model materials in scalable amounts. Consequently, research efforts are now shifting towards establishing critical structure-viscoelasticity relationships. Inspired by previous achievements in the field of dynamic polymer networks, we believe that the use of more sophisticated network models offers one pathway towards success in this goal. Deep understanding of vitrimer flow and processability can only be achieved through a union of rigorous synthesis, experimental characterization, and modeling.

Supporting Information

(i) δ versus temperature for PDMS, and (ii) temperature dependence of PS viscosity showing non-Arrhenius behavior.

Acknowledgments

This work is based in part upon work supported by the National Science Foundation under grant no. NSF DMR-1727870 (SS). We also acknowledge Florida State University and the FAMU-FSU College of Engineering for support.

References

(1) Montarnal, D.; Capelot, M.; Tournilhac, F.; Leibler, L. Silica-like malleable materials from permanent organic networks. *Science* **2011**, *334*, 965–968, DOI: 10.1126/science.1212648.

(2) Scheutz, G. M.; Lessard, J. J.; Sims, M. B.; Sumerlin, B. S. Adaptable crosslinks in poly-

meric materials: Resolving the intersection of thermoplastics and thermosets. *J. Am. Chem. Soc.* **2019**, *141*, 16181–16196, DOI: 10.1021/jacs.9b07922.

(3) Winne, J. M.; Leibler, L.; Du Prez, F. E. Dynamic covalent chemistry in polymer networks: a mechanistic perspective. *Polym. Chem.* **2019**, *10*, 6091–6108, DOI: 10.1039/C9PY01260E.

(4) Guerre, M.; Taplan, C.; Winne, J. M.; Du Prez, F. E. Vitrimers: Directing chemical reactivity to control material properties. *Chem. Sci.* **2020**, *11*, 4855–4870, DOI: 10.1039/d0sc01069c.

(5) Van Zee, N. J.; Nicolaÿ, R. Vitrimers: Permanently crosslinked polymers with dynamic network topology. *Prog. Polym. Sci.* **2020**, *104*, 101233, DOI: 10.1016/j.progpolymsci.2020.101233.

(6) Parada, G. A.; Zhao, X. Ideal reversible polymer networks. *Soft Matter* **2018**, *14*, 5186–5196, DOI: 10.1039/C8SM00646F.

(7) Zhang, Y.; Broekhuis, A. A.; Picchioni, F. Thermally self-healing polymeric materials: the next step to recycling thermoset polymers? *Macromolecules* **2009**, *42*, 1906–1912, DOI: 10.1021/ma8027672.

(8) Scott, T. F.; Schneider, A. D.; Cook, W. D.; Bowman, C. N. Photoinduced plasticity in crosslinked polymers. *Science* **2005**, *308*, 1615–1617, DOI: 10.1126/science.1110505.

(9) Röttger, M.; Domenech, T.; van der Weegen, R.; Breuillac, A.; Nicolaÿ, R.; Leibler, L. High-performance vitrimers from commodity thermoplastics through dioxaborolane metathesis. *Science* **2017**, *356*, 62–65, DOI: 10.1126/science.aah5281.

(10) Nishimura, Y.; Chung, J.; Muradyan, H.; Guan, Z. Silyl ether as a robust and thermally stable dynamic covalent motif for malleable polymer design. *J. Am. Chem. Soc.* **2017**, *139*, 14881–14884, DOI: 10.1021/jacs.7b08826.

(11) Demongeot, A.; Groote, R.; Goossens, H.; Hoeks, T.; Tournilhac, F.; Leibler, L. Cross-linking of poly(butylene terephthalate) by reactive extrusion using Zn(II) epoxy-vitrimer chemistry. *Macromolecules* **2017**, *50*, 6117–6127, DOI: 10.1021/acs.macromol.7b01141.

(12) Ricarte, R. G.; Tournilhac, F.; Leibler, L. Phase separation and self-assembly in vitrimers: Hierarchical morphology of molten and semicrystalline polyethylene/dioxaborolane maleimide systems. *Macromolecules* **2019**, *52*, 432–443, DOI: 10.1021/acs.macromol.8b02144.

(13) Ricarte, R. G.; Tournilhac, F.; Clotre, M.; Leibler, L. Linear viscoelasticity and flow of self-assembled vitrimers: the case of a polyethylene/dioxaborolane system. *Macromolecules* **2020**, *53*, 1852–1866, DOI: 10.1021/acs.macromol.9b02415.

(14) He, C.; Shi, S.; Wu, X.; Russell, T. P.; Wang, D. Atomic force microscopy nanomechanical mapping visualizes interfacial broadening between networks due to chemical exchange reactions. *J. Am. Chem. Soc.* **2018**, *140*, 6793–6796, DOI: 10.1021/jacs.8b03771.

(15) Lessard, J. J.; Garcia, L. F.; Easterling, C. P.; Sims, M. B.; Bentz, K. C.; Arencibia, S.; Savin, D. A.; Sumerlin, B. S. Catalyst-free vitrimers from vinyl polymers. *Macromolecules* **2019**, *52*, 2105–2111, DOI: 10.1021/acs.macromol.8b02477.

(16) Lessard, J. J.; Scheutz, G. M.; Hughes, R. W.; Sumerlin, B. S. Polystyrene-based vitrimers: inexpensive and recyclable thermosets. *ACS Appl. Polym. Mater.* **2020**, *2*, 3044–3048, DOI: 10.1021/acsapm.0c00523.

(17) Taplan, C.; Guerre, M.; Winne, J. M.; Du Prez, F. E. Fast processing of highly crosslinked, low-viscosity vitrimers. *Mater. Horiz.* **2020**, *7*, 104–110, DOI: 10.1039/c9mh01062a.

(18) Capelot, M.; Unterlass, M. M.; Tournilhac, F.; Leibler, L. Catalytic control of the vitrimer glass transition. *ACS Macro Lett.* **2012**, *1*, 789–792, DOI: 10.1021/mz300239f.

(19) Capelot, M.; Montarnal, D.; Tournilhac, F.; Leibler, L. Metal-catalyzed transesterification for healing and assembling of thermosets. *J. Am. Chem. Soc.* **2012**, *134*, 7664–7667, DOI: 10.1021/ja302894k.

(20) Capelot, M. Chimie de polycondensation, polymères supramoléculaires et vitrimères. Ph.D. thesis, Université Pierre et Marie Curie - Paris VI, 2013.

(21) Denissen, W.; Rivero, G.; Nicolaÿ, R.; Leibler, L.; Winne, J. M.; Du Prez, F. E. Vinylogous urethane vitrimers. *Adv. Funct. Mater.* **2015**, *25*, 2451–2457, DOI: 10.1002/adfm.201404553.

(22) Röttger, M. Associative exchange reactions of boron or nitrogen containing bonds and design of vitrimers. Theses, Université Pierre et Marie Curie - Paris VI, 2016.

(23) Hendriks, B.; Waelkens, J.; Winne, J. M.; Du Prez, F. E. Poly(thioether) vitrimers via transalkylation of trialkylsulfonium salts. *ACS Macro Lett.* **2017**, 930–934, DOI: 10.1021/acsmacrolett.7b00494.

(24) Ishibashi, J. S. A.; Kalow, J. A. Vitrimeric silicone elastomers enabled by dynamic meldrum's acid-derived cross-links. *ACS Macro Letters* **2018**, *7*, 482–486, DOI: 10.1021/acsmacrolett.8b00166.

(25) He, C.; Shi, S.; Wang, D.; Helms, B. A.; Russell, T. P. Poly(oxime-ester) vitrimers with catalyst-free bond exchange. *J. Am. Chem. Soc.* **2019**, *141*, 13753–13757, DOI: 10.1021/jacs.9b06668.

(26) El-Zaatari, B. M.; Ishibashi, J. S. A.; Kalow, J. A. Cross-linker control of vitrimer flow. *Polym. Chem.* **2020**, DOI: 10.1039/d0py00233j.

(27) Brutman, J. P.; Delgado, P. A.; Hillmyer, M. A. Polylactide vitrimers. *ACS Macro Lett.* **2014**, *3*, 607–610, DOI: 10.1021/mz500269w.

(28) Altuna, F. I.; Hoppe, C. E.; Williams, R. J. Shape memory epoxy vitrimers based on DGEBA crosslinked with dicarboxylic acids and their blends with citric acid. *RSC Adv.* **2016**, *6*, 88647–88655, DOI: 10.1039/c6ra18010h.

(29) Stukenbroeker, T.; Wang, W.; Winne, J. M.; Du Prez, F. E.; Nicola, R.; Leibler, L. Polydimethylsiloxane quenchable vitrimers. *Polym. Chem.* **2017**, *8*, 6590–6593, DOI: 10.1039/C7PY01488K.

(30) Altuna, F. I.; Hoppe, C. E.; Williams, R. J. J. Epoxy vitrimers: the effect of transesterification reactions on the network structure. *Polymers* **2018**, *10*, 43, DOI: 10.3390/polym10010043.

(31) Poutrel, Q.-A.; Blaker, J.; Soutis, C.; Tournilhac, F.; Gresil, M. Dicarboxylic acid-epoxy vitrimers: Influence of off-stoichiometric acid content on cure reactions and thermo-mechanical properties. *Polym. Chem.* **2020**, *11*, 5327–5338, DOI: 10.1039/d0py00342e.

(32) Denissen, W.; Droesbeke, M.; Nicolaÿ, R.; Leibler, L.; Winne, J. M.; Du Prez, F. E.; Nicola, R.; Leibler, L.; Winne, J. M.; Du Prez, F. E. Chemical control of the viscoelastic properties of vinylogous urethane vitrimers. *Nat. Commun.* **2017**, *8*, 14857, DOI: 10.1038/ncomms14857.

(33) Self, J. L.; Dolinski, N. D.; Zayas, M. S.; Read De Alaniz, J.; Bates, C. M. Brønsted-acid-catalyzed exchange in polyester dynamic covalent networks. *ACS Macro Lett.* **2018**, *7*, 817–821, DOI: 10.1021/acsmacrolett.8b00370.

(34) Demongeot, A.; Mougnier, S. J.; Okada, S.; Soulié-Ziakovic, C.; Tournilhac, F. Coordination and catalysis of Zn^{2+} in epoxy-based vitrimers. *Polym. Chem.* **2016**, *7*, 4486–4493, DOI: 10.1039/c6py00752j.

(35) Fortman, D. J.; Brutman, J. P.; Cramer, C. J.; Hillmyer, M. A.; Dichtel, W. R. Mechani-

cally activated, catalyst-free polyhydroxyurethane vitrimers. *J. Am. Chem. Soc.* **2015**, *137*, 14019–14022, DOI: 10.1021/jacs.5b08084.

(36) Snyder, R. L.; Fortman, D. J.; De Hoe, G. X.; Hillmyer, M. A.; Dichtel, W. R. Reprocessable acid-degradable polycarbonate vitrimers. *Macromolecules* **2018**, *51*, 389–397, DOI: 10.1021/acs.macromol.7b02299.

(37) Lu, Y.-x. X.; Tournilhac, F.; Leibler, L.; Guan, Z. Making insoluble polymer networks malleable via olefin metathesis. *J. Am. Chem. Soc.* **2012**, *134*, 8424–8427, DOI: 10.1021/ja303356z.

(38) Breuillac, A.; Kassalias, A.; Nicolaÿ, R. Polybutadiene vitrimers based on dioxaborolane chemistry and dual networks with static and dynamic cross-links. *Macromolecules* **2019**, *52*, 7102–7113, DOI: 10.1021/acs.macromol.9b01288.

(39) He, C.; Christensen, P. R.; Seguin, T. J.; Dailing, E. A.; Wood, B. M.; Walde, R. K.; Persson, K. A.; Russell, T. P.; Helms, B. A. Conformational entropy as a means to control the behavior of poly(diketoenamine) vitrimers in and out of equilibrium. *Angew. Chemie - Int. Ed.* **2020**, *59*, 735–739, DOI: 10.1002/anie.201912223.

(40) Zhou, Y.; Goossens, J. G.; Sijbesma, R. P.; Heuts, J. P. Poly(butylene terephthalate)/glycerol-based vitrimers via solid-state polymerization. *Macromolecules* **2017**, *50*, 6742–6751, DOI: 10.1021/acs.macromol.7b01142.

(41) Zhou, Y.; Goossens, J. G.; van den Bergen, S.; Sijbesma, R. P.; Heuts, J. P. In situ network formation in PBT vitrimers via processing-induced deprotection chemistry. *Macromol. Rapid Commun.* **2018**, *39*, 1800356, DOI: 10.1002/marc.201800356.

(42) Zhou, Y.; Groote, R.; Goossens, J. G.; Sijbesma, R. P.; Heuts, J. P. Tuning PBT vitrimer properties by controlling the dynamics of the adaptable network. *Polym. Chem.* **2019**, *10*, 136–144, DOI: 10.1039/c8py01156g.

(43) Li, L.; Chen, X.; Jin, K.; Torkelson, J. M. Vitrimers designed both to strongly suppress creep and to recover original cross-link density after reprocessing: Quantitative theory and experiments. *Macromolecules* **2018**, *51*, 5537–5546, DOI: 10.1021/acs.macromol.8b00922.

(44) Meng, F.; Saed, M. O.; Terentjev, E. M. Elasticity and relaxation in full and partial vitrimer networks. *Macromolecules* **2019**, *52*, 7423–7429, DOI: 10.1021/acs.macromol.9b01123.

(45) Saed, M. O.; Gablier, A.; Terentjev, E. M. Liquid crystalline vitrimers with full or partial boronic-ester bond exchange. *Adv. Funct. Mater.* **2020**, *30*, 1906458, DOI: 10.1002/adfm.201906458.

(46) Self, J. L.; Sample, C. S.; Levi, A. E.; Li, K.; Xie, R.; de Alaniz, J. R.; Bates, C. M. Dynamic bottlebrush polymer networks: self-healing in super-soft materials. *J. Am. Chem. Soc.* **2020**, *142*, 7567–7573, DOI: 10.1021/jacs.0c01467.

(47) Chen, X.; Li, L.; Wei, T.; Torkelson, J. M. Reprocessable polymer networks designed with hydroxyurethane dynamic cross-links: Effect of backbone structure on network morphology, phase segregation, and property recovery. *Macromol. Chem. Phys.* **2019**, *220*, 1900083, DOI: 10.1002/macp.201900083.

(48) Lessard, J. J.; Scheutz, G. M.; Sung, S. H.; Lantz, K. A.; Epps, T. H.; Sumerlin, B. S. Block copolymer vitrimers. *J. Am. Chem. Soc.* **2020**, *142*, 283–289, DOI: 10.1021/jacs.9b10360.

(49) Altuna, F. I.; Casado, U.; Dell'Erba, I. E.; Luna, L.; Hoppe, C. E.; Williams, R. J. J. Epoxy vitrimers incorporating physical crosslinks produced by self-association of alkyl chains. *Polym. Chem.* **2020**, *11*, 1337–1347, DOI: 10.1039/C9PY01787A.

(50) Yang, Y.; Pei, Z.; Zhang, X.; Tao, L.; Wei, Y.; Ji, Y. Carbon nanotube-vitrimer compos-

ite for facile and efficient photo-welding of epoxy. *Chem. Sci.* **2014**, *5*, 3486–3492, DOI: 10.1039/c4sc00543k.

(51) Legrand, A.; Soulié-Ziakovic, C. Silica-epoxy vitrimer nanocomposites. *Macromolecules* **2016**, *49*, 5893–5902, DOI: 10.1021/acs.macromol.6b00826.

(52) Chabert, E.; Vial, J.; Cauchois, J. P.; Mihaluta, M.; Tournilhac, F. Multiple welding of long fiber epoxy vitrimer composites. *Soft Matter* **2016**, *12*, 4838–4845, DOI: 10.1039/c6sm00257a.

(53) Yan, P.; Zhao, W.; Jiang, L.; Wu, B.; Hu, K.; Yuan, Y.; Lei, J. Reconfiguration and shape memory triggered by heat and light of carbon nanotubepolyurethane vitrimer composites. *J. Appl. Polym. Sci.* **2018**, *135*, 45784, DOI: 10.1002/app.45784.

(54) Spiesschaert, Y.; Taplan, C.; Stricker, L.; Guerre, M.; Winne, J. M.; Du Prez, F. E. Influence of the polymer matrix on the viscoelastic behaviour of vitrimers. *Polym. Chem.* **2020**, *11*, 5377–5385, DOI: 10.1039/D0PY00114G.

(55) Snijkers, F.; Pasquino, R.; Maffezzoli, A. Curing and viscoelasticity of vitrimers. *Soft Matter* **2017**, *13*, 258–268, DOI: 10.1039/C6SM00707D.

(56) Wu, S.; Yang, H.; Huang, S.; Chen, Q. Relationship between reaction kinetics and chain dynamics of vitrimers based on dioxaborolane metathesis. *Macromolecules* **2020**, *53*, 1180–1190, DOI: 10.1021/acs.macromol.9b02162.

(57) Hayashi, M.; Yano, R.; Takasu, A. Synthesis of amorphous low T_g polyesters with multiple cooh side groups and their utilization for elastomeric vitrimers based on post-polymerization cross-linking. *Polym. Chem.* **2019**, *10*, 2047–2056, DOI: 10.1039/C9PY00293F.

(58) Pritchard, R. H.; Redmann, A.-L. L.; Pei, Z.; Ji, Y.; Terentjev, E. M. Vitrification and plastic flow in transient elastomer networks. *Polymer* **2016**, *95*, 45–51, DOI: 10.1016/j.polymer.2016.04.060.

(59) Meng, F.; Pritchard, R. H.; Terentjev, E. M. Stress relaxation, dynamics, and plasticity of transient polymer networks. *Macromolecules* **2016**, *49*, 2843–2852, DOI: 10.1021/acs.macromol.5b02667.

(60) Meng, F.; Terentjev, E. Transient network at large deformations: Elastic-plastic transition and necking instability. *Polymers* **2016**, *8*, 108, DOI: 10.3390/polym8040108.

(61) Long, R.; Qi, H. J.; Dunn, M. L. Modeling the mechanics of covalently adaptable polymer networks with temperature-dependent bond exchange reactions. *Soft Matter* **2013**, *9*, 4083–4096, DOI: 10.1039/c3sm27945f.

(62) Ma, J.; Mu, X.; Bowman, C. N.; Sun, Y.; Dunn, M. L.; Qi, H. J.; Fang, D. A photoviscoplastic model for photoactivated covalent adaptive networks. *J. Mech. Phys. Solids* **2014**, *70*, 84–103, DOI: 10.1016/j.jmps.2014.05.008.

(63) Yu, K.; Shi, Q.; Wang, T.; Dunn, M. L.; Jerry Qi, H. A computational model for surface welding in covalent adaptable networks using finite-element analysis. *J. Appl. Mech.* **2016**, *83*, 1–11, DOI: 10.1115/1.4033682.

(64) Yu, K.; Shi, Q.; Li, H.; Jabour, J.; Yang, H.; Dunn, M. L.; Wang, T.; Qi, H. J. Interfacial welding of dynamic covalent network polymers. *J. Mech. Phys. Solids* **2016**, *94*, 1–17, DOI: 10.1016/j.jmps.2016.03.009.

(65) Sun, X.; Wu, H.; Long, R. Thermomechanics of a temperature sensitive covalent adaptable polymer with bond exchange reactions. *Soft Matter* **2016**, *12*, 8847–8860, DOI: 10.1039/c6sm01857b.

(66) Luo, C.; Shi, X.; Lei, Z.; Zhu, C.; Zhang, W.; Yu, K. Effects of bond exchange reactions and relaxation of polymer chains on the thermomechanical behaviors of covalent adaptable network polymers. *Polymer* **2018**, *153*, 43–51, DOI: 10.1016/j.polymer.2018.08.001.

(67) Jourdain, A.; Asbai, R.; Anaya, O.; Chehimi, M. M.; Drockenmuller, E.; Montarnal, D. Rheological properties of covalent adaptable networks with 1,2,3-triazolium cross-links: the missing link between vitrimers and dissociative networks. *Macromolecules* **2020**, *53*, 1884–1900, DOI: 10.1021/acs.macromol.9b02204.

(68) Fang, H.; Fang, H.; Fang, H.; Ye, W.; Ding, Y.; Ding, Y.; Winter, H. H. Rheology of the critical transition state of an epoxy vitrimer. *Macromolecules* **2020**, *53*, 4855–4862, DOI: 10.1021/acs.macromol.0c00843.

(69) Perego, A.; Khabaz, F. Volumetric and rheological properties of vitrimers: a hybrid molecular dynamics and Monte Carlo simulation study. *Macromolecules* **2020**, *53*, 8406–8416, DOI: 10.1021/acs.macromol.0c01423.

(70) Smallenburg, F.; Leibler, L.; Sciortino, F. Patchy particle model for vitrimers. *Phys. Rev. Lett.* **2013**, *111*, 188002, DOI: 10.1103/PhysRevLett.111.188002.

(71) Rovigatti, L.; Nava, G.; Bellini, T.; Sciortino, F. Self-dynamics and collective swap-driven dynamics in a particle model for vitrimers. *Macromolecules* **2018**, *51*, 1232–1241, DOI: 10.1021/acs.macromol.7b02186.

(72) Ciarella, S.; Sciortino, F.; Ellenbroek, W. G. Dynamics of vitrimers: Defects as a highway to stress relaxation. *Phys. Rev. Lett.* **2018**, *121*, 058003, DOI: 10.1103/PhysRevLett.121.058003.

(73) Shivokhin, M. E.; Narita, T.; Talini, L.; Habicht, A.; Seiffert, S.; Indei, T.; Schieber, J. D. Interplay of entanglement and association effects on the dynamics of semidilute solutions of multisticker polymer chains. *J. Rheol.* **2017**, *61*, 1231–1241, DOI: 10.1122/1.4997740.

(74) Green, M. S.; Tobolsky, A. V. A new approach to the theory of relaxing polymeric media. *J. Chem. Phys.* **1946**, *14*, 80–92, DOI: 10.1063/1.1724109.

(75) Yamamoto, M. The visco-elastic properties of network structure I. General formalism. *J. Phys. Soc. Jpn.* **1956**, *11*, 413–421, DOI: 10.1143/JPSJ.11.413.

(76) Lodge, A. A network theory of flow birefringence and stress in concentrated polymer solutions. *Trans. Faraday Soc.* **1956**, *52*, 120–130.

(77) Tanaka, F.; Edwards, S. F. Viscoelastic properties of physically crosslinked networks. 1. Transient network theory. *Macromolecules* **1992**, *25*, 1516–1523, DOI: 10.1021/ma00031a024.

(78) Wientjes, R. H. W.; Jongschaap, R. J. J.; Duits, M. H. G.; Mellema, J. A new transient network model for associative polymer networks. *J. Rheol.* **1999**, *43*, 375–391, DOI: 10.1122/1.551039.

(79) Indei, T.; Takimoto, J.-i. Linear viscoelastic properties of transient networks formed by associating polymers with multiple stickers. *J. Chem. Phys.* **2010**, *133*, 194902, DOI: 10.1063/1.3498779.

(80) Baxandall, L. G. Dynamics of reversibly crosslinked chains. *Macromolecules* **1989**, *22*, 1982–1988, DOI: 10.1021/ma00194a076.

(81) Rouse, P. R. A theory of the linear viscoelastic properties of dilute solutions of coiling polymers. *J. Chem. Phys.* **1953**, *21*, 1272–1280.

(82) Leibler, L.; Rubinstein, M.; Colby, R. H. Dynamics of reversible networks. *Macromolecules* **1991**, *24*, 4701–4707, DOI: 10.1021/ma00016a034.

(83) Leibler, L.; Rubinstein, M.; Colby, R. H. Dynamics of telechelic ionomers. Can polymers diffuse large distances without relaxing stress? *J. Phys. II* **1993**, *3*, 1581–1590, DOI: 10.1051/jp2:1993219.

(84) Rubinstein, M.; Semenov, A. N. Thermoreversible gelation in solutions of associating polymers. 2. Linear dynamics. *Macromolecules* **1998**, *31*, 1386–1397, DOI: 10.1021/ma970617+.

(85) Rubinstein, M.; Semenov, A. N. Dynamics of entangled solutions of associating polymers. *Macromolecules* **2001**, *34*, 1058–1068, DOI: 10.1021/ma0013049.

(86) Chen, Q.; Tudryn, G. J.; Colby, R. H. Ionomer dynamics and the sticky Rouse model. *J. Rheol.* **2013**, *57*, 1441–1462, DOI: 10.1122/1.4818868.

(87) Zhang, Z.; Chen, Q.; Colby, R. H. Dynamics of associative polymers. *Soft Matter* **2018**, *14*, 2961–2977, DOI: 10.1039/C8SM00044A.

(88) Tripathi, A.; Tam, K. C.; McKinley, G. H. Rheology and dynamics of associative polymers in shear and extension: Theory and experiments. *Macromolecules* **2006**, *39*, 1981–1999, DOI: 10.1021/ma051614x.

(89) Ahmadi, M.; Hawke, L. G. D.; Goldansaz, H.; van Ruymbeke, E. Dynamics of entangled linear supramolecular chains with sticky side groups: Influence of hindered fluctuations. *Macromolecules* **2015**, *48*, 7300–7310, DOI: 10.1021/acs.macromol.5b00733.

(90) Hawke, L. G. D.; Ahmadi, M.; Goldansaz, H.; van Ruymbeke, E. Viscoelastic properties of linear associating poly(n-butyl acrylate) chains. *J. Rheol.* **2016**, *60*, 297–310, DOI: 10.1122/1.4942231.

(91) Spruijt, E.; Cohen Stuart, M. A.; Van Der Gucht, J. Linear viscoelasticity of polyelectrolyte complex coacervates. *Macromolecules* **2013**, *46*, 1633–1641, DOI: 10.1021/ma301730n.

(92) Syed, V. M.; Srivastava, S. Time-ionic strength superposition: A unified description of chain relaxation dynamics in polyelectrolyte complexes. *ACS Macro Letters* **2020**, *9*, 1067–1073, DOI: 10.1021/acsmacrolett.0c00252.

(93) Morin, F. J.; Puppo, M. L.; Laaser, J. Decoupling salt- and polymer-dependent dynamics in polyelectrolyte complex coacervates via salt addition. 2020; https://chemrxiv.org/articles/preprint/Decoupling_Salt-_and_Polymer-Dependent_Dynamics_in_Polyelectrolyte_Complex_Coacervates_via_Salt_Addition/12469556/1.

(94) Tang, S.; Wang, M.; Olsen, B. D. Anomalous self-diffusion and sticky Rouse dynamics in associative protein hydrogels. *J. Am. Chem. Soc.* **2015**, *137*, 3946–3957, DOI: 10.1021/jacs.5b00722.

(95) Bird, R.; Armstrong, R.; Hassager, O. *Dynamics of polymeric liquids, Vol. 1, Fluid mechanics*; John Wiley& Sons: New York, 1987.

(96) Larson, R. G. *Constitutive equations for polymer melts and solutions*; Butterworth-Heinemann, 1988; DOI: https://doi.org/10.1016/C2013-0-04284-3.

(97) Doi, M.; Edwards, S. F. *The theory of polymer dynamics*; Clarendon Press: Oxford, 1986.

(98) Provencher, S. W. An eigenfunction expansion method for the analysis of exponential decay curves. *J. Chem. Phys.* **1976**, *64*, 2772–2777, DOI: 10.1063/1.432601.

(99) Baumgaertel, M.; Winter, H. H. Determination of discrete relaxation and retardation time spectra from dynamic mechanical data. *Rheol. Acta* **1989**, *28*, 511–519, DOI: 10.1007/BF01332922.

(100) Takeh, A.; Shanbhag, S. A computer program to extract the continuous and discrete relaxation spectra from dynamic viscoelastic measurements. *Appl. Rheol.* **2013**, *23*, 24628.

(101) Shanbhag, S. pyReSpect: A computer program to extract discrete and continuous spectra from stress relaxation experiments. *Macromol. Theory Simul.* **2019**, 1900005, DOI: 10.1002/mats.201900005.

(102) Shanbhag, S. Relaxation spectra using nonlinear Tikhonov regularization with a Bayesian criterion. *Rheol. Acta* **2020**, *59*, 509–520, DOI: 10.1007/s00397-020-01212-w.

(103) Hansen, D. R.; Shen, M. Viscoelastic retardation time computations for homogeneous block copolymers. *Macromolecules* **1975**, *8*, 343–348, DOI: 10.1021/ma60045a020.

(104) Stockmayer, W. H.; Kennedy, J. W. Viscoelastic spectrum of free-draining block copolymers. *Macromolecules* **1975**, *8*, 351–355, DOI: 10.1021/ma60045a022.

(105) Wang, F. W.; DiMarzio, E. A. The dynamics of block-copolymer molecules in solution. The free-draining limit. *Macromolecules* **1975**, *8*, 356–360, DOI: 10.1021/ma60045a023.

(106) Rubinstein, M.; Helfand, E.; Pearson, D. S. Theory of polydispersity effects of polymer rheology: Binary distribution of molecular weights. *Macromolecules* **1987**, *20*, 822–829, DOI: 10.1021/ma00170a021.

(107) Jiang, N.; Zhang, H.; Tang, P.; Yang, Y. Linear viscoelasticity of associative polymers: Sticky Rouse model and the role of bridges. *Macromolecules* **2020**, *53*, 3438–3451, DOI: 10.1021/acs.macromol.0c00312.

(108) Dean, P. Vibrations of glass-like disordered chains. *Proc. Phys. Soc.* **1964**, *84*, 727–744, DOI: 10.1088/0370-1328/84/5/310.

(109) Chen, Q.; Liang, S.; Shiau, H.-s.; Colby, R. H. Linear viscoelastic and dielectric properties of phosphonium siloxane ionomers. *ACS Macro Lett.* **2013**, *2*, 970–974, DOI: 10.1021/mz400476w.

(110) Laidler, K. J. The development of the Arrhenius equation. *J. Chem. Educ.* **1984**, *61*, 494, DOI: 10.1021/ed061p494.

(111) Colby, R. H.; Zheng, X.; Rafailovich, M. H.; Sokolov, J.; Peiffer, D. G.; Schwarz, S. A.; Strzhemechny, Y.; Nguyen, D. Dynamics of lightly sulfonated polystyrene ionomers. *Phys. Rev. Lett.* **1998**, *81*, 3876–3879, DOI: 10.1103/PhysRevLett.81.3876.

(112) Criado, J.; Pérez-Maqueda, L.; Sánchez-Jiménez, P. Dependence of the preexponential factor on temperature. *J. Therm. Anal. Calorim.* **2005**, *82*, 671–675.

(113) Oeser, R.; Ewen, B.; Richter, D.; Farago, B. Dynamic fluctuations of crosslinks in a rubber: a neutron-spin-echo study. *Phys. Rev. Lett.* **1988**, *60*, 1041–1044, DOI: 10.1103/PhysRevLett.60.1041.

(114) Williams, M. L.; Landel, R. F.; Ferry, J. D. The temperature dependence of relaxation mechanisms in amorphous polymers and other glass-forming liquids. *J. Am. Chem. Soc.* **1955**, *77*, 3701–3707, DOI: 10.1021/ja01619a008.

(115) Ferry, J. *Viscoelastic properties of polymers*, 3^{rd} ed.; John Wiley & Sons Inc: Hoboken, NY, 1980.

(116) Fuchs, K.; Friedrich, C.; Weese, J. Viscoelastic properties of narrow-distribution poly(methyl methacrylates). *Macromolecules* **1996**, *29*, 5893–5901, DOI: 10.1021/ma951385m.

(117) Zhang, Z.; Huang, C.; Weiss, R. A.; Chen, Q. Association energy in strongly associative polymers. *J. Rheol.* **2017**, *61*, 1199–1207, DOI: 10.1122/1.4997586.

(118) de Gennes, P. G. Kinetics of diffusioncontrolled processes in dense polymer systems. I. Nonentangled regimes. *J. Chem. Phys.* **1982**, *76*, 3316–3321, DOI: 10.1063/1.443328.

(119) Brassinne, J.; Cadix, A.; Wilson, J.; van Ruymbeke, E. Dissociating sticker dynamics from chain relaxation in supramolecular polymer networks – The importance of free partner! *J. Rheol.* **2017**, *61*, 1123–1134, DOI: 10.1122/1.4997594.

(120) Gold, B. J.; Hvelmann, C. H.; Lhmann, N.; Szkely, N. K.; Pyckhout-Hintzen, W.; Wischnewski, A.; Richter, D. Importance of compact random walks for the rheology of transient networks. *ACS Macro Lett.* **2017**, *6*, 73–77, DOI: 10.1021/acsmacrolett.6b00880.

(121) Stukalin, E. B.; Cai, L.-H.; Kumar, N. A.; Leibler, L.; Rubinstein, M. Self-healing of unentangled polymer networks with reversible bonds. *Macromolecules* **2013**, *46*, 7525–7541, DOI: 10.1021/ma401111n.

(122) Schapery, R.; Park, S. Methods of interconversion between linear viscoelastic material functions. Part II – an approximate analytical method. *Int. J. Solids Struct.* **1999**, *36*, 1677 – 1699, DOI: https://doi.org/10.1016/S0020-7683(98)00060-2.

(123) Loy, R. J.; de Hoog, F. R.; Anderssen, R. S. Interconversion of Prony series for relaxation and creep. *J. Rheol.* **2015**, *59*, 1261–1270, DOI: 10.1122/1.4929398.

(124) Flory, P. J.; Rehner, J. Statistical mechanics of crossLinked polymer networks I. Rubberlike elasticity. *J. Chem. Phys.* **1943**, *11*, 512–520, DOI: 10.1063/1.1723791.

(125) Flory, P. J. Molecular size distribution in three dimensional polymers. I. Gelation. *J. Am. Chem. Soc.* **1941**, *63*, 3083–3090, DOI: 10.1021/ja01856a061.

(126) Stockmayer, W. H. Theory of molecular size distribution and gel formation in branched polymers II. General cross linking. *J. Chem. Phys.* **1944**, *12*, 125–131, DOI: 10.1063/1.1723922.

(127) Zhou, H.; Woo, J.; Cok, A. M.; Wang, M.; Olsen, B. D.; Johnson, J. A. Counting primary loops in polymer gels. *Proc. Natl. Acad. Sci.* **2012**, *109*, 19119–19124, DOI: 10.1073/pnas.1213169109.

(128) Schieber, J. D.; Andreev, M. Entangled polymer dynamics in equilibrium and flow modeled through slip links. *Ann. Rev. Chem. Biomol. Engg.* **2014**, *5*, 367–381, DOI: 10.1146/annurev-chembioeng-060713-040252.

(129) Masubuchi, Y. Simulating the flow of entangled polymers. *Ann. Rev. Chem. Biomol. Engg.* **2014**, *5*, 11–33, DOI: 10.1146/annurev-chembioeng-060713-040401, PMID: 24498953.

(130) Shanbhag, S. Fast slip link model for bidisperse linear polymer melts. *Macromolecules* **2019**, *52*, 3092–3103, DOI: 10.1021/acs.macromol.8b02367.

(131) Müller, M.; Dardin, A.; Seidel, U.; Balsamo, V.; Iván, B.; Spiess, H. W.; Stadler, R. Junction dynamics in telechelic hydrogen bonded polyisobutylene networks. *Macromolecules* **1996**, *29*, 2577–2583, DOI: 10.1021/ma950984q.

(132) Adzima, B. J.; Aguirre, H. A.; Kloxin, C. J.; Scott, T. F.; Bowman, C. N. Rheological and chemical analysis of reverse gelation in a covalently cross-linked Diels-Alder polymer network. *Macromolecules* **2008**, *41*, 9112–9117, DOI: 10.1021/ma801863d, PMID: 20711364.

(133) Stadler, F. J.; Pyckhout-Hintzen, W.; Schumers, J.-M.; Fustin, C.-A.; Gohy, J.-F.; Bailly, C. Linear viscoelastic rheology of moderately entangled telechelic polybutadiene temporary networks. *Macromolecules* **2009**, *42*, 6181–6192, DOI: 10.1021/ma802488a.

(134) Weiss, R. A.; Zhao, H. Rheological behavior of oligomeric ionomers. *J. Rheol.* **2009**, *53*, 191–213, DOI: 10.1122/1.3003570.

Graphical TOC Entry